Rap2 and TNIK control Plexin-dependent synaptic tiling in *C. elegans*

Xi Chen[1,], Akihiro C. E. Shibata[2,4], Ardalan Hendi[1,4], Mizuki Kurashina[1], Ethan Fortes[1], Nicholas L Weilinger[3], Brian MacVicar[3], Hideji Murakoshi[2] and Kota Mizumoto[1]

Author affiliations:

1. Department of Zoology, The University of British Columbia, Vancouver, Canada.

2. Supportive Center for Brain Research, National Institute for Physiological Sciences, Okazaki, Aichi, Japan.

3. Department of Cellular and Physiological Sciences, The University of British Columbia, Vancouver, Canada.

4. These authors contributed equally to this work

Correspondence

Kota Mizumoto

mizumoto@zoology.ubc.ca

1-604-827-0794

Department of Zoology, The University of British Columbia

2350 Health Sciences Mall, LSC2406, Vancouver, BC, V6T 1Z3, Canada

Abstract

During development, neurons form synapses with their fate-determined targets. While we begin to elucidate the mechanisms by which extracellular ligand-receptor interactions enhance synapse specificity by inhibiting synaptogenesis, our knowledge about their intracellular mechanisms remains limited. Here we show that Rap2 GTPase (*rap-2*) and its effector, TNIK (*mig-15*), act downstream of Plexin (*plx-1*) to restrict presynaptic assembly and to form tiled synaptic innervation in *C. elegans*. Both constitutively GTP- and GDP-forms of *rap-2* mutants exhibit synaptic tiling defects as *plx-1* mutants, suggesting that cycling of the RAP-2 nucleotide state is critical for synapse inhibition. Consistently, RAP-2 activity is locally suppressed by PLX-1. Excessive ectopic synapse formation in *mig-15* mutants causes a severe synaptic tiling defect. Conversely, overexpression of *mig-15* strongly inhibited synapse formation, suggesting that *mig-15* is a negative regulator of synapse formation. These results reveal that subcellular regulation of small GTPase activity by Plexin shapes proper synapse patterning in vivo.

Introduction

During nervous system development, various instructive and repulsive signaling cues cooperatively direct neurons to form chemical synapses with their appropriate targets. Studies have identified some molecules and elucidated their downstream mechanisms that instruct synaptogenesis such as FGF, Ephrin/Eph, Ig-family of cell adhesion molecules (IgCAMs) and synaptic cell adhesion molecules (SynCAMs) (Shen and Bargmann, 2003; Shen et al., 2004). Several axon guidance cues and their receptors also play critical roles to inhibit synapse formation (Inaki et al., 2007). Semaphorins (Sema) and their receptors, Plexins, are two conserved families of molecules that have a well-established function to repel axons during development (Kolodkin et al., 1993; 1992; Negishi et al., 2005; Tran et al., 2007) and prominent roles contributing to immune system, cardiovascular development and cancer regulation (Epstein et al., 2015; Neufeld et al., 2005; Takamatsu and Kumanogoh, 2012).

In addition to its function as a long-range axon guidance cue during neuronal development, Sema/Plexin signaling plays a critical role as a negative regulator of synapse formation. The role of Sema/Plexin signaling in inhibiting synapse formation was first observed in Drosophila, where ectopic expression of Sema-2a causes elimination of specific neuromuscular junctions (Matthes et al., 1995). In mammals, Sema3E/PlexinD1 specifies sensory-motor connections (Pecho-Vrieseling et al., 2009). Secreted Sema3F locally inhibits spine development through its receptors PlexinA3 and Neuropilin-2 in hippocampal granule cells (Tran et al., 2009), and Sema5A/PlexinA2 signaling inhibits excitatory synapse formation in dentate granule cells (Duan et al., 2014). Sema5B diminishes synaptic connections in cultured hippocampal neurons (O'Connor et al., 2009). However, little is known about the intracellular mechanisms through which Sema/Plexin signaling inhibits synapse formation.

The cytoplasmic domain of Plexin contains a GAP (GTPase-activating protein) domain that inactivates small GTPases (Oinuma et al., 2004; Rohm et al., 2000). Upon activation by Semaphorins, Plexins repel axon outgrowth by inhibiting R-Ras (Negishi et al., 2005). Recent biochemical and structural analyses demonstrated the GAP domain of mammalian PlexinA3 is specific for Rap GTPases, which belong to the Ras family of GTPases and regulate actin cytoskeleton (Wang et al., 2012; 2013). PlexinA3 dimerization by Semaphorin activates its GAP domain, thereby inhibiting Rap1 from inducing neurite retraction. Drosophila PlexA and zebrafish PlexinA1 promote remodeling of epithelial cells by inhibiting Rap1 GTPase during wound healing (Yoo et al., 2016). Another Rap GTPase, Rap2, can inhibit neurite outgrowth (Kawabe et al., 2010). Similar to Sema/Plexin signaling, Rap GTPases regulate synapse formation and function. Rap2 negatively regulate spine number in cultured hippocampal neurons (Fu et al., 2007). Rap1 and Rap2 regulate synaptic activity by removing AMPA receptors from spines during long-term depression and depotentiation, respectively (J. J. Zhu et al., 2002; Y. Zhu et al., 2005). While the GAP domain of Plexin is critical to inhibit synapse formation (Duan et al., 2014; Mizumoto and Shen, 2013a), we still do not know whether Plexin regulates synapse patterning via Rap GTPases at presynaptic sites.

In *Caenorhabditis elegans*, Sema/Plexin signaling functions in vulva formation and male ray development (Dalpé et al., 2005; 2004; Fujii et al., 2002; Ikegami et al., 2004; Liu et al., 2005; Nakao et al., 2007; Nukazuka et al., 2008; 2011). Using this model system, we previously reported that Sema/Plexin signaling in the nervous system mediates a critical inter-axonal interaction for the tiled synaptic innervation of two DA-class cholinergic motor neurons (DA8 and DA9) (Mizumoto and Shen, 2013a). Cell bodies of nine DA neurons in *C. elegans* reside in the ventral nerve cord, sending dendrites ventrally and axons dorsally to form *en passant* synapses onto the

dorsal body wall muscles. Even though axons of DA neurons show significant overlap, each motor neuron forms synapses onto muscles within specific sub-axonal domains, which do not overlap with those from neighboring DA neurons. This unique synaptic innervation creates tiled synaptic patterns along the nerve cord (White et al., 1986).

Tiled synaptic innervation occurs within most motor neuron classes and may contribute to the sinusoidal locomotion pattern of *C. elegans* (White et al., 1986). Using a combination of two fluorescent proteins (GFP and mCherry) fused with the presynaptic vesicle protein, RAB-3, and two tissue specific promoters (Figure 1) (Mizumoto and Shen, 2013a), we can visualize this synaptic tiling between DA8 and DA9 neurons. We reported that PLX-1 localizes at the anterior edge of the DA9 synaptic domain in axon-axon interactions in a Semaphorin-dependent manner, where it locally inhibits formation of the presynaptic specialization via its GAP domain. Loss of *Semas* or *plx-1* causes anterior expansion of DA9 synaptic domain and posterior expansion of DA8 synaptic domain. This result indicates loss of inter-axonal interactions between DA8 and DA9 neurons. Consistently, Tran et al., also observed excess dendritic spine formation, specifically within the region close to the cell body, in the *plexin* knockout mouse (Tran et al., 2009). These findings suggest a conserved mechanism by which Sema/Plexin locally inhibits synapse formation.

We previously reported that *let-60/KRas* gain-of-function mutants showed mild synaptic tiling defects. Since mammalian Plexin acts as a RapGAP and very mild synaptic tiling defects of *let-60(gf)* mutants, we hypothesized that Rap GTPase is the major downstream effector of PLX-1 to regulate synaptic tiling of DA neurons. Here, we report that *rap-2*, a *C. elegans* ortholog of human Rap2A, and its effector kinase *mig-15* (TNIK: Traf2- and Nck-interacting kinase) act downstream of PLX-1 to regulate synaptic tiling. *plx-1* delineates the border of synaptic tiling by locally inhibiting *rap-2* along the DA9 axon. We also found an unexpected role of *mig-15* in

inhibiting synapse formation. Our results reveal the molecular mechanism underlying Plexin signaling to form fine synaptic map connectivity.

Results

rap-2 functions downstream of *plx-1* to regulate synaptic tiling

Three Rap genes exist in the *C. elegans* genome (*rap-1*, *rap-2* and *rap-3*). To delineate which Rap GTPase functions downstream of PLX-1 in synaptic tiling between DA8 and DA9 neurons, we first examined the expression patterns of all three *rap* genes (Figures S1). Among them, only *rap-2*, an ortholog of mammalian Rap2a, was expressed in motor neurons including DA8 and DA9, while *rap-1* and *rap-3* were not expressed in these cells (Figures S1A-C). In wild type animals, synaptic domains of DA8 and DA9 neurons did not show significant overlap, creating tiled synaptic innervation (Figures 1A and 1G). In the *plx-1(nc36)* null mutant, synaptic domains of DA8 and DA9 expanded posteriorly and anteriorly, respectively. As a result, synaptic domains of these neurons overlapped significantly (Figures 1B and 1G).

Since the intracellular domain of Plexin contains a RapGAP domain, we hypothesized that RAP-2 preferentially exists in a GTP-bound form in the *plx-1* mutants. The G12V mutant is widely used as a constitutively GTP-form of small GTPases including mammalian Rap2A and *C. elegans* RAP-1 (Kawabe et al., 2010; Pellis-van Berkel et al., 2005). Expression of a constitutively GTP-bound form of *rap-2(G12V)* under the A-type neuron specific promoter, P*unc-4*, elicited a similar synaptic tiling defect as *plx-1* mutants (Figures 1C and 1G). Expression of wild type *rap-2* under the *unc-4* promoter did not affect the synaptic tiling pattern, suggesting that G12V mutation but not over-expression of *rap-2* caused the synaptic tiling defect (Figure 1G). We then generated *rap-2(G12V)* mutants using CRISPR/Cas9 genome editing. We observed the same synaptic tiling

defects in three independent *rap-2(G12V)* mutant alleles (*miz16*, *miz17* and *miz18*) as in *plx-1* mutants (Figures 1D, 1G and S2). We found a comparable level of gene expression among all three *rap-2(G12V)* mutants to wild type *rap-2* using RT-qPCR(Figure S2B). These results confirm that the *rap-2(G12V)* mutation itself, not changes in gene expression, underlie the synaptic tiling defect in *rap-2(G12V)* mutants.

Surprisingly, the null mutant of *rap-2(gk11)* also showed the same synaptic tiling defect, as did the constitutively GTP-form of *rap-2(G12V)* mutants (Figures 1E and 1G). This result suggests that synaptic tiling requires both the GTP- and GDP-bound forms of RAP-2. Indeed, the constitutively GDP-bound form of *rap-2* mutants (S17A: *miz19*, *miz20*) showed the identical synaptic tiling defect as *rap-2(G12V)* and *rap-2(gk11)* mutants (Figures 1F, 1G and Figure S2). These results suggest that the cycling between GTP- and GDP-forms of RAP-2 is critical to regulate the spatial patterning of synapses.

Similar to *plx-1* mutants, the synaptic tiling defect in all *rap-2* mutants is caused by both the posterior expansion of DA8 synaptic domain and the anterior expansion of the DA9 synaptic domain (Figures S2C and S2D). However, none of *rap-2(G12V)*, *rap-2(S17A)* and *rap-2(gk11)* mutants enhanced or suppressed the synaptic tiling defect in *plx-1* mutants (Figure 1G). These results suggest that *plx-1* and *rap-2* function in the same genetic pathway. Consistent with the expression patterns of *rap-1* and *rap*-3, neither *rap-1(pk2082)* nor *rap-3(gk3975)* null mutants showed significant synaptic tiling defects by themselves and did not enhance the synaptic tiling defect in *rap-2(gk11)* null mutants (Figures S1D-G). All mCherry::RAB-3 puncta co-localized with active zone markers, CLA-1 (Xuan et al., 2017) and UNC-10/Rim (Wu et al., 2013) in the DA9 neurons of *plx-1(nc36)* and *rap-2(gk11)* mutants, suggesting that RAB-3 puncta represent

bona fide synapses (Figure S3). Taken together, these data indicate that *plx-1* and *rap-2* act in the same genetic pathway for synaptic tiling in DA neurons.

RAP-2 functions cell autonomously in DA neurons

We next determined the cellular location for *rap-2* function. Since *rap-2(gk11)* null mutants showed a synaptic tiling defect, we conducted tissue specific rescue experiments using tissue-specific promoters as previously described (Mizumoto and Shen, 2013a). Expression of *rap-2* in the post-synaptic body wall muscle cells under the *hlh-1* promoter or in another class of cholinergic motor neurons in the dorsal nerve cord (DB neurons) under the truncated *unc-129* promoter did not rescue the synaptic tiling defect in *rap-2(gk11)* animals (Figures 2A, 2B and 2G). However, DA neuron-specific expression using the *unc-4c* promoter strongly rescued the synaptic tiling defect (Figures 2C and 2G). DA9-specific expression of *rap-2* under the *mig-13* promoter partially rescued the synaptic tiling defect (Figures 2E and 2G). DA9-specific expression of *rap-2* rescued the phenotype of anterior expansion of the DA9 synaptic domain but not the posterior expansion of DA8 synaptic domain (Figures 2H and 2I). These results suggest that *rap*-2 regulates synapse patterning in a cell-autonomous manner. In contrast to the DA9-specific rescue experiment in *rap-2* mutants, DA9-specific expression of *plx-1* cDNA was sufficient to rescue synaptic defects in both DA9 and DA8 (Mizumoto and Shen, 2013a) (see discussion).

We also observed that expression of human Rap2a in DA neurons rescued the synaptic tiling defect of *rap-2* mutants, suggesting the function of *rap-2* in synapse patterning is conserved across species (Figures 2D and 2G). Previous work suggested a partial functional redundancy between *rap-1* and *rap*-2 in *C. elegans* (Pellis-van Berkel et al., 2005). However, we found that *rap-1* expression in DA neurons did not rescue the synaptic tiling defect of *rap-2* mutants,

suggesting functional diversity between *rap-1* and *rap*-2 (Figures 2F and 2G). Taken together, we conclude that *rap-2* functions cell autonomously in DA neurons to regulate synaptic tiling.

RAP-2 activity is spatially regulated by PLX-1

Previously, we demonstrated that PLX-1::GFP is localized at the anterior edge of the DA9 synaptic domain, where it negatively regulates synapse formation through its cytoplasmic GAP domain (Figures 3A and 3E) (Mizumoto and Shen, 2013a). In the *rap-2(gk11)* mutant background, we observed no change in PLX-1::GFP localization but did observe ectopic synapses in the axonal region anterior to the PLX-1::GFP domain (Figures 3B and 3F). This result is consistent with our hypothesis that *rap-2* acts downstream of *plx-1* to regulate synaptic tiling. Together with our findings that synaptic tiling requires both GTP- and GDP-bound forms of RAP-2, we speculate that PLX-1 acting at the anterior edge of the DA9 synaptic domain regulates the spatial activity of RAP-2 along the axon.

We then sought to determine the spatial distribution of GTP-RAP-2 in DA9 axons. We conducted Fluorescence Lifetime Imaging Microscopy (FLIM)-based FRET (Förster Resonance Energy Transfer) measurements using EGFP-Rap2A (human) and mRFP-RalGDS(RBD: Ras Binding Domain)-mRFP (Yasuda et al., 2006). As RalGDS-RBD specifically binds to GTP-Rap2 but not GDP-Rap2 (Ohba et al., 2000), FRET from EGFP-Rap2A to mRFP-RalGDS(RBD)-mRFP can be used as a readout of Rap2 activity. We detected FRET signal as a change of GFP fluorescence lifetime (Figure 4A). In HeLa cells, we observed a shorter lifetime of constitutively bound GTP construct EGFP-Rap2A(G12V) compared to GDP-bound EGFP-Rap2A(S17A), indicating that the FRET sensor can detect the nucleotide state of Rap2A (Figures 4B and 4C).

Due to the low expression of *C. elegans* RAP-2 constructs in HeLa cells, we were not able to test whether the mammalian FRET sensor can detect *C. elegans* RAP-2 activity (data not shown).

We then expressed EGFP-Rap2A and mRFP-RalGDS(RBD)-mRFP FRET sensors in DA9 neurons in *C. elegans*. As human Rap2a rescued the synaptic tiling defect of *rap-2(gk11)* mutants (Figure 2G), we reasoned that the activity pattern of human Rap2A should recapitulate that of endogenous RAP-2. We indeed observed lower Rap2A activity at the anterior edge of the DA9 synaptic domain compared to within the synaptic domain (Figures 4D and 4F). This observation is consistent with the localization of PLX-1::GFP at the anterior edge of DA9 synaptic domain (Figure 3A) (Mizumoto and Shen, 2013a). Local inhibition of Rap2a activity was strongly diminished in the *plx-1* mutant background (Figures 4D and 4F). Higher Rap2 activity in the synaptic region could be simply due to the presence of synapses within the synaptic domain, rather than Rap2 inactivation by Plexin at the anterior edge of the synaptic domain. To exclude this possibility, we examined the Rap2 activity in *unc-104/Kif1A* mutants in which no synapses are formed in DA9 axon (Ou et al., 2010). We showed previously that PLX-1::GFP localization to the synaptic tiling border was independent of synapses since it was unaffected in *unc-104/Kif1A* mutants (Mizumoto and Shen, 2013a). In *unc-104* mutants, we observed the same local inhibition of Rap2A activity at the putative synaptic tiling border, but not in *unc-104; plx-1* double mutants (Figures 4E and 4G), indicating that Plexin controls local Rap2 activity independent of synapses.

To understand that this local Rap2 inactivation at the synaptic tiling border depends on the localized RapGAP activity of PLX-1, we examined the rescue activity of two PLX-1 mutant constructs, PLX-1(RA) and PLX-1(ΔSema), neither of which rescued the synaptic tiling defect of *plx-1* mutants (Mizumoto and Shen, 2013a). PLX-1(RA) is a GAP-deficient mutant but localizes normally at the anterior edge of the DA9 synaptic domain. PLX-1(ΔSema) contains intact GAP

domain but cannot be activated by the ligand and shows diffused localization due to the deletion of the extracellular SEMA domain (Mizumoto and Shen, 2013a). We observed no local Rap2 inactivation in *plx-1* mutant animals expressing these mutant PLX-1 constructs in DA9, while expression of wild type PLX-1 cDNA rescued the local Rap2 inactivation at the anterior edge of DA9 synaptic domain (Figure 4H).

While we do not fully exclude the possibility that PLX-1 indirectly regulates local Rap2 activity, together with the biochemical evidence that mammalian Plexin acts as RapGAP (Wang et al., 2013; 2012), these data strongly suggests that Plexin localized at the anterior edge of the DA9 synaptic domain locally inactivates Rap2 GTPase to delineate the synaptic tiling border in DA9.

mig-15(*TNIK*) regulates synaptic tiling

In mammals, TNIK (Traf2 and Nck1-interacting kinase) acts with Rap2 to regulate neurite extension and AMPA receptor trafficking in hippocampal neurons and microvilli formation in intestinal cells (Hussain et al., 2010; Kawabe et al., 2010). In *C. elegans*, *mig-15* is the sole ortholog of mammalian TNIK and its paralog MINK1 (Misshapen-like kinase 1), which is also an effector of Rap GTPase (Nonaka et al., 2008). *mig-15* can regulate various cellular processes, such as axon guidance and cell migration (Chapman et al., 2008; Poinat et al., 2002; Shakir et al., 2006; Teulière et al., 2011). We found that *mig-15(rh148)* hypomorphic mutants showed a severe synaptic tiling defect (Figures 5A and 5D). Similar to *plx-1* and *rap-2* mutants, the synaptic tiling defect followed the anterior expansion of the DA9 synaptic domain and the posterior expansion of the DA8 synaptic domain (Figures 5E and 5F). All RAB-3 puncta in *mig-15(rh148)* mutants are co-localized with active zone markers, CLA-1 and UNC-10 (Figure S3), suggesting that these

RAB-3 puncta represent bona fide synapses. We observed axon guidance defects (23%, n=100) or ectopic branch formation (56%, n=100) in DA9 of *mig-15* mutant animals (Figure S4). These were excluded from our analysis of synaptic tiling phenotypes. Whereas only half of the *mig-15* mutant animals showed guidance defects or ectopic branch formation, the synaptic tiling defect of *mig-15* mutants was almost fully penetrant (Figure 5D). We did not observe significant synaptic tiling defects in *cdh-4(rh310)* mutants (DA8/DA9 overlap: 4.6 ±1.02 μm, n=21), which exhibits axon defasciculation phenotype in the dorsal nerve cord neurons (Schmitz et al., 2008). These data suggest that the synaptic tiling defect in the *mig-15* mutants is not a secondary effect of axon outgrowth and guidance.

The other two nonsense alleles (*rh326: Q439Stop*, *rh80: W898Stop*) also showed identical synaptic tiling defects as *mig-15(rh148)* (Figures S5A-5E). *mig-15(rh80)* has a nonsense mutation within the highly conserved CNH (citron/NIK homology) domain, which is required to interact with Rap2 in both mammals and *C. elegans* (Taira et al., 2004). This suggests a physical interaction between RAP-2 and MIG-15 for synaptic tiling. *plx-1* or *rap-2* mutants did not enhance the synaptic tiling defect in *mig-15* mutants (Figures 5B-5F). This result is consistent with the hypothesis that *mig-15* acts in the same genetic pathway as *plx-1* and *rap-2*. The PLX-1::GFP patch at the putative synaptic tiling border was unaffected in *mig-15* mutants, even though the position of the PLX-1::GFP patch has shifted slightly posteriorly compared with wild type (Figures 3C and 3G), suggesting that *mig-15* acts downstream of PLX-1 in regulating synaptic tiling.

Interestingly, the degree of overlap between DA8 and DA9 synaptic domains was even larger in *mig-15* mutants than those observed in *plx-1* and *rap-2* mutants (compare Figures 1G

and 5D). Taken together, these results suggest that *mig-15* also acts downstream of additional signaling pathways (see discussion).

mig-15 functions in DA neurons

We then sought to determine in which cells *mig-15* functions by conducting tissue specific rescue experiments. Since several *mig-15* isoforms (wormbase and data not shown) exist, we used the *mig-15* genomic sequence for the rescue experiments. Expression of *mig-15* under the DA neuron specific promoter (*Punc-4c*) strongly rescued the synaptic tiling defect of *mig-15(rh148)* mutants (Figures 6A and 6F), consistent with our hypothesis that *mig-15* acts in the same genetic pathway as *plx-1* and *rap-2*.

Expression of *mig-15* in both DA8 and DA9 rescued both posterior expansion of the DA8 synaptic domain and anterior expansion of the DA9 synaptic domain (Figures 6G and 6H). DA9 specific expression of *mig-15* under the *mig-13* promoter rescued anterior expansion of the DA9 synaptic domain, suggesting that *mig-15* functions cell autonomously in DA9 (Figures 6B and 6G). We observed that P*mig-13::mig-15* weakly rescued the posterior expansion of the DA8 synaptic domain (Figure 6H). This is likely due to the leaky expression of *mig-15* in DA8, as the *mig-15* genomic fragment without promoter showed slight rescue of the synaptic tiling defect in *mig-15(rh148)* mutants (Figure 6F). Kinase dead TNIK mutants act as a dominant-negative (Mahmoudi et al., 2009). Expression of mutant *mig-15(kd)*, which carries the same mutation at the corresponding amino acid of the dominant-negative TNIK (Figure 6E), in DA neurons caused a severe synaptic tiling defect (Figures 6C, 6D and 6I). Based on these results, we conclude that *mig-15* functions cell autonomously in DA neurons.

mig-15 inhibits synapse formation

We observed that DA9-specific expression of *mig-15* under the *mig-13* promoter in *mig-15* mutants often exhibited a shorter synaptic domain compared to wild type (Figures 6B and 6G). So, we speculated that an excess amount of *mig-15* inhibits synapse formation. We tested the effect of *mig-15* overexpression in the wild type background. Strikingly, DA9-specific *mig-15* overexpression in wild type (*mig-15(OE)*) significantly reduced synapse number compared to wild type (Figures 7A, 7C, 7D and S6). This reduction occurred without affecting overall morphology of the DA9 neuron (Figure S4). Conversely, DA9 synapse number was significantly increased in the *mig-15(rh148)* mutants (Figures 7B, 7D and S6).

Similarly, *mig-15* overexpression significantly reduced synapse number in DD-type GABAergic motor neurons (Figure S7). These results indicate that *mig-15* is a negative regulator of synapse formation. Furthermore, pan-neuronal expression of *mig-15* under the *rab-3* promoter caused severe uncoordinated locomotion in wildtype animals (Figure S8). These locomotor defects occurred concomitant with significantly reduced GFP::RAB-3 intensity in the dorsal nerve cord in *mig-15* over-expressing animals and without causing significant axon guidance defects (Figure S8). Taken together, these data indicate that reduced synapse number by *mig-15* overexpression disrupted the proper functioning of the motor circuit.

Importantly, we observed no significant increase in synapse numbers in *plx-1* or *rap-2* mutants (Figure S6), suggesting that the role of *mig-15* in negatively regulating synapse number is independent of its role in PLX-1/RAP-2 -mediated synaptic tiling (Figure 8G).

Rap GTPase and TNIK are well-known actin cytoskeleton regulators (Lin et al., 2010; 2008; Taira et al., 2004). Previous studies demonstrated that ARP2/3-dependent branched F-actin is required for presynaptic development (P. Chia et al., 2012; P. H. Chia et al., 2014). Branched F-

actin visualized by GFP::ut-CH (utrophin calponin homology domain) is enriched within the DA9 synaptic domain (Figure 7E) (P. Chia et al., 2012; Mizumoto and Shen, 2013a). We predicted that *mig-15* negatively regulates synapse formation by re-organizing the branched F-actin at the anterior edge of the synaptic domain. Consistently, we observed longer synaptic F-actin distribution in *rap-2(gk11)* and *mig-15(rh148)* mutants (Figures 7F, 7G and 7I). While GFP::utCH was observed in the posterior asynaptic axonal region or in the dendrite of DA9, synapse formation is likely inhibited by Wnt and Netrin signaling as reported previously (Klassen and Shen, 2007; Poon et al., 2008). Conversely, overexpression of *mig-15* in DA9 significantly decreased the length of synaptic F-actin (Figures 7H and 7I). Overexpression of *mig-15* also appeared to decrease the overall amount of synaptic F-actin (Figure 7H). This result suggests that *mig-15* inhibits synapse formation by negatively regulating the formation of synaptic F-actin.

plx-1 and *rap-2* can coordinate the position of synaptic tiling border and synapse number

mig-15(OE) caused a reduction of synapse number in DA9. As a result, the length of DA9 synaptic domain was significantly reduced in *mig-15(OE)* animals than in wild type (Figures 8A and 8E). Despite this, synaptic tiling is maintained without a significant gap between DA8 and DA9 synaptic domains in *mig-15(OE)* animals, suggesting that the position of synaptic tiling border has shifted posteriorly in *mig-15(OE)* animals. Indeed, the length of the posterior asynaptic domain of DA8 was significantly shorter in *mig-15(OE)* animals, indicating that the DA8 synaptic domain expanded posteriorly (Figure 8D). Furthermore, the PLX-1::GFP patch at the anterior edge of the DA9 synaptic domain shifted posteriorly in *mig-15(OE)* animals with reduced synapse number (Figure 3D). These results strongly suggest that the PLX-1/RAP-2 signaling pathway can specify the position of synaptic tiling border according to the available number of synapses in each

DA neuron (Figure 8G). It is therefore likely that synaptic tiling is a mechanism to maintain the uniform distribution of the synapses from one class of motor neuron in the nerve cord. Consistently, DA8 synaptic domain did not shift posteriorly when *mig-15* was overexpressed in DA9 of the synaptic tiling mutants, *plx-1* or *rap-2* (Figures 8B-8D). This result suggests that DA8 no longer senses the reduction of DA9 synapse number in the synaptic tiling mutants. Synapse number was not different between *mig-15(OE)* and in *rap-2(gk11); mig-15(OE)* animals (Figure S6), suggesting that the role of *mig-15* in inhibiting synapse number is not dependent on Plexin/Rap2 signaling pathway (Figure 8G).

In summary, we demonstrate that synaptic tiling is a mechanism to maintain a uniform distribution of synapses from one class of motor neurons along the nerve cord. Further, our results indicate *plx-1* and *rap-2* play critical roles in this process by coordinating the position of the synaptic tiling border.

Discussion

While much is known about the morphogenic triggers for axon guidance and patterned synapse formation, the downstream sequelae of these intracellular effectors has remained unclear. We discovered the role of Rap2 GTPase and TNIK in synapse pattern formation in *C. elegans*. Since Sema/Plexin signaling processes to inhibit synapse formation are well conserved across species, we propose that Sema/Plexin also utilize Rap2 and TNIK to regulate synapse patterning in mammals as well.

Cell autonomous and non-autonomous functions of Sema/Plexin signaling components

Previously we showed that both *smp-1* and *plx-1* are necessary and sufficient in DA9, which suggests that *smp-1* and *plx-1* act cell-autonomously in DA9 and non-autonomously in DA8 to determine the synaptic tiling border. We proposed that Sema/PLX-1 in DA9 send a retrograde signal to DA8 through an unidentified signaling molecule (X) to induce the synaptic tiling pattern in DA8 (Mizumoto and Shen, 2013a). However, we found that both *rap-2* and *mig-15* act cell autonomously, since our DA9-specific rescue experiment only rescued the DA9 phenotype, but not the DA8 phenotype. This conclusion is further supported since the synaptic tiling defects of these mutants were fully rescued when both neurons express functional *rap-2* cDNA or *mig-15* genomic DNA. We propose that each neuron utilizes a different set of cell surface proteins but share common intracellular mechanisms to specify synapse patterning. Diverse signaling and cell adhesion molecules, such as atrial natriuretic peptide receptor (NPR) and GPCRs, regulate Rap activity (Birukova et al., 2008; Gloerich and Bos, 2011; Weissman et al., 2004). Screening for these potential Rap regulators should identify novel molecules that interact with Sema/Plexin and act in DA9.

Cycling of Rap GTPase activity in synaptic tiling

We showed that both GDP- and GTP-forms of RAP-2 are required for proper synapse patterning. Considering that PLX-1 regulates the spatial distribution of RAP-2 activity and *mig-15* acts downstream of *rap-2* in synaptic tiling, RAP-2 may also locally regulate MIG-15(TNIK). While we did not observe a specific subcellular localization of GFP-MIG-15 in DA9 (data not shown), PLX-1 and RAP-2 may instead regulate MIG-15 activity rather than its spatial localization. Further biochemical characterization of MIG-15 regulation by GTP-RAP-2 or GDP-RAP-2 will be necessary to understand the exact functions of RAP-2 in synapse patterning.

Small GTPase activity is regulated by GAP and GEF (Guanine nucleotide exchange factor) proteins. Yet, we did not observe significant synaptic tiling defects in mutants of putative RAP-2 GEFs, which include *pxf-1(RAPGEF2/6)* and *epac-1(RAPGEF3/4/5)* (data not shown) (Frische et al., 2007; Pellis-van Berkel et al., 2005). We speculate that multiple RapGEFs act redundantly to activate RAP-2 in synaptic tiling.

mig-15(TNIK) may integrate multiple inhibitory cues during synapse formation

mig-15 mutants show a greater degree of overlap between DA8 and DA9 synaptic domains than *plx-1* or *rap-2* mutants. This effect partially occurs from excess synaptogenesis in the posterior asynaptic domain of both DA8 and DA9 neurons. Previously, we demonstrated that Wnt morphogens and their receptors, Frizzled, instruct synaptic topographic patterning by locally inhibiting synapse formation. Indeed, synaptic tiling defects in *mig-15* mutants was somewhat similar to the combined effect of *plx-1* and *wnt* mutants (Mizumoto and Shen, 2013b). TNIK can act as a positive regulator of the canonical Wnt signaling pathway in colorectal cancer cells (Mahmoudi et al., 2009). While we do not know whether the canonical Wnt signaling pathway contributes to local inhibition of synapse formation, we propose that TNIK integrates multiple signaling pathways for precise synapse pattern formation.

In addition to its role in synapse pattern formation, our data indicate that *mig-15* also plays a role as a negative regulator of synapse number. Since neither *plx-1* nor *rap-2* mutants showed significant increase in synapse number in DA9, *mig-15* seems to inhibit synapse formation in a different signaling pathway (Figure 8G). Since we observed global reduction of synaptic actin staining in animals over-expressing *mig-15*, it is likely that *mig-15* controls synapse number via regulating synaptic F-actin.

The exact mechanisms of synaptic actin regulation by TNIK remain undetermined. TNIK could activate JNK kinase pathway (Taira et al., 2004). The MIG-15/JNK-1 signaling pathway inhibits axonal branch formation in sensory neurons in *C. elegans* (Crawley et al., 2017). In contrast to these well-established role of MIG-15/TNIK as an activator of the JNK pathway, we did not observe any synaptic tiling defect in *jnk-1* mutant animals (Figure S5F and S5G). Our result suggests *mig-15* does not inhibit synapse formation through the JNK pathway. Further genetic studies of *mig-15* in synaptic tiling will elucidate the molecular mechanisms that underlie the role of MIG-15/TNIK in synapse pattern formation and in decreasing synapse number.

Plexin signaling and diseases

Aberrant neuronal wiring underlies many neurological disorders. Not surprisingly, Semaphorin and Plexin genes are associated with various neurodevelopmental disorders and intellectual disabilities, including autism spectrum disorders (ASD) and schizophrenia (Mah et al., 2006). For example, PLXNB1, SEMA3A, SEMA4D and SEMA6C are significantly upregulated in the prefrontal cortices of schizophrenic patients (Eastwood et al., 2003). However, non-synonymous variations in the Sema3D gene had a significant protective effect against developing schizophrenia (Fujii et al., 2011). More recent work showed that loss of Sema5A/PlexA2 signaling induces excess excitatory synapse formation in granule cells, which causes ASD-like behavioural defects in mice (Duan et al., 2014).

Similar to Sema/Plexin signaling, TNIK is also associated with various neurological disorders, including schizophrenia and intellectual disabilities (Anazi et al., 2016; Potkin et al., 2010). TNIK can also physically bind and act with DISC1 (Disrupted in Schizophrenia 1) to regulate synaptic composition (Q. Wang et al., 2011). So, we propose that the

Sema/Plexin/Rap2/TNIK signaling pathway plays a critical role to precisely define synaptic connections and its disruption may induce serious neurological disorders.

Interestingly, SNPs in Plexin genes are also associated with extremely high IQ. Recent work suggests that loss of PlexinA1 confers better motor control in rodents, due to increased synaptic connectivity in the corticospinal cord (Gu et al., 2017; Spain et al., 2016). Further studies on the Plexin/Rap2/TNIK signaling pathway in synapse map formation, as presented here, will likely reveal the genetic basis of these disorders and conditions.

Methods

Strains

All *C. elegans* strains were derived from Bristol N2 and raised on OP50 *Escherichia coli*-seeded nematode growth medium (NGM) plates at 20 C and maintained as described previously (Brenner, 1974). The following mutants were used in this study: *unc-104(e1265)II, plx-1(nc36)IV, rap-1(pk2082)IV, rap-3(gk3975)IV, jnk-1(gk7)IV rap-2(gk11)V, rap-2(miz16)V, rap-2(miz17)V, rap-2(miz18)V, rap-2(miz19)V. rap-2(miz20)V, mig-15(rh148)X, mig-15(rh80)X, mig-15(rh326)X.*

CRISPR/Cas9 genome editing

rap-2(miz16)V, rap-2(miz17)V, rap-2(miz18)V, rap-2(miz19)V. rap-2(miz20)V were generated using Co-CRISPR method (Kim et al., 2014). *unc-22* or *dpy-10* co-CRISPR markers were used for selecting candidate animals (Arribere et al., 2014; Kim et al., 2014). Vectors for sgRNA and Cas9 were obtained from Addgene (Plasmid ID: 46169 and 46168, respectively) (Friedland et al., 2013). The *rap-2* guide RNA sequence (5' – gTAGTGGAGGTGTCGGAAAAT-3') was designed using MIT CRISPR design tool (crispr.mit.edu:8079) and inserted into sgRNA vector using Q5 Site-Directed Mutagenesis kit (NEB). Repair templates with either G12V (*miz17* and *miz18*) and S17A (*miz19* and *miz20*) mutation were generated by PCR with primer sets carrying corresponding mutations (see supplemental Experimental Procesures). Synonymous mutations were also introduced in the sgRNA recognition sequence to avoid Cas9 recruitment to the edited genome. PCR products were cloned into *Eco*RI site of the pBluescript SK(+) vector. Synthesized double-stranded DNA (GeneArt, Thermo Fisher) was used as a repair template for generating *rap-2(miz16)* mutant.

Plasmid constructions

C. elegans expression clones were made in a derivative of pPD49.26 (A. Fire), the pSM vector (kind gift from S. McCarroll and C. I. Bargmann). Primer sets used in this study are listed in the Supplemental Experimental Procedures. The following constructs were used and transgenes were generated using standard microinjection method (Mello et al., 1991): *wyIs446 (Punc-4::2xGFP-rab-3; Pmig-13::mCherry-rab-3; Podr-1::RFP), wyIs85 (Pitr-1::GFP-rab-3; Podr-1::RFP), wyIs442 (Pflp-13::2xGFP-rab-3; Pplx-2::mCherry-rab-3; Podr-1::RFP), wyIs320 (Pitr-1::plx-1::GFP; Pmig-13::mCherry;;rab-3; Podr-1::GFP), wyIs329 (Pmig-13::GFP-utCH; Pmig-13::mCherry::rab-3; Podr-1::GFP), wyIs524 (Punc-4::2xGFP-rab-3; Pmig-13::mCherry-rab-3; Podr-1::RFP), wyIs685 (Pmig-13::mCherry::rab-3; Pmig-13::GFPnovo2::cla-1; Podr-1::GFP) mizIs1 (Pitr-1::GFPnovo2-CAAX; Pvha-6::zif-1; Pitr-1::mCherry::rab-3; Podr-1::GFP), mizIs19 (Pmig-13::eGFP::hRap2a; Pmig-13::mRFP-RalGDS(RBD)-mRFP; Podr-1::GFP), mizIs33 (Prab-3::mig-15; Podr-1::GFP), jsIs682 (Prab-3::GFP::rab-3; lin-15(+)), wyEx5445 (Prap-1::GFP; Punc-4::myr-mCherry; Podr-1::RFP), wyEx5464 (Prap-2::GFP; Punc-4::myr-mCherry; Podr-1::RFP), mizEx194 (Prap-3::GFP; Pmig-13::myr-mCherry; Podr-1::RFP), mizEx165 (Phlh-1::rap-2; Podr-1::GFP), mizEx164 (Punc-129::rap-2; Podr-1::GFP), mizEx174 (Punc-4c::rap-2; Podr-1::GFP), mizEx157 (Pmig-13::rap-2; Podr-1::GFP), mizEx156 (Punc-4c::hRap2a; Podr-1::GFP), mizEx177 (Punc-4c::rap-1; Podr-1::GFP), mizEx151 (Pmig-13::mig-15; Podr-1::GFP), mizEx147 (Punc-4c::mig-15; Podr-1::GFP), mizEx153 (ΔpSMmig-15; Podr-1::GFP), mizEx178 (Punc-4c::mig-15(K50A); Podr-1::GFP), mizEx173 (Punc-4::rap-2(G12V); Podr-1::GFP), mizEx179 (Pflp-13::mig-15; Podr-1::GFP), mizEx170 (Pmig-13::mig-15; Podr-1::GFP), mizEx197 (Pmig-13::mig-15; Podr-1::GFP), mizEx210 (Pmig-13::mig-15; Podr-1::RFP), mizEx257 (Prab-3::GFP; Prab-3::mCherry::rab-3, Podr-1::mScarlet::CAAX), mizEx272 (Podr-1::GFP; Pmig-13::unc-10::TdTomato); mizEx309 (Pmig-13::plx-1(RA); Podr-*

1::RFP), mizEx312 (Pmig-13::plx-1(Δsema); Podr-1::RFP); mizEx314 (Pmig-13::plx-1; Podr-1::RFP).

Cloning of *rap-1*, *rap-2* and *mig-15*

cDNAs of *rap-1* and *rap-2* were obtained from cDNA library prepared from N2 RNA. Trizol (Invitrogen) was used to purify total RNA from N2, and the SuperScript III First-Strand Synthesis System for RT-PCR (Invitrogen) was used for the reverse-transcription. *mig-15* genomic DNA was amplified from the N2 genomic DNA purified using GeneJET Genomic DNA Purification Kit (Thermo Scientific). Phusion (NEB) or Q5 (NEB) DNA polymerases were used for all PCR reactions for amplifying cDNA and genomic DNA fragments. Amplified fragments were cloned into the *Asc*I and *Kpn*I sites of pSM vector using SLiCE method (Motohashi, 2015), Gibson assembly (Gibson et al., 2009) or T4 ligase (NEB). List of primers used in this study is available in the Supplemental Experimental Procedures.

Confocal Microscopy

Images of fluorescently tagged fusion proteins were captured in live *C. elegans* using a Zeiss LSM800 confocal microscope (Carl Zeiss, Germany). Worms were immobilized on 2% agarose pad using a mixture of 7.5 mM levamisole (Sigma-Aldrich) and 0.225M BDM (2,3-butanedione monoxime) (Sigma-Aldrich). Images were analyzed with Zen software (Carl Zeiss) or Image J (NIH, USA). Definition of each parameter is as follows (Mizumoto and Shen, 2013a): DA8/9 overlap: a distance between the most anterior DA9 synapse and the most posterior DA8 synapse, DA8 asynaptic domain: a distance from commissure to the most posterior DA8 synapse, DA9 synaptic domain: a distance between the most anterior and posterior DA9 synapses. Middle L4 (judged by the stereotyped shape of developing vulva) animals were used for quantification.

Averages were taken from at least 20 samples. For GFP::Utrophin-CH, we measured the length from the posterior end of dorsal axon to the anterior end of GFP::Utrophin-CH domain. For each marker strain, the same imaging setting (laser power, gain pinhole) and image processing were used for comparing different genotypes.

Two-photon FLIM-FRET experiment

Expression vector for cultured cells (pCI-eGFP-hRap2a, pCI-eGFP-RAP-1, pCI-eGFP-RAP-2, pCI-eGFP-RAP-2(G12V), pCI-eGFP-RAP-2(S17A)) were generated by replacing Ras in pCI-eGFP-Ras (Yasuda et al., 2006) with hRap2a and *rap-2* cDNAs with *Xho*I and *Bam*HI. pCI-mRFP-RalGDS-mRFP plasmid is a kind gift from Dr. Yasuda. Rap2 and FRET sensor plasmids were mixed in 1:2 ratio and transfected into HeLa cells using Lipofectamine 3000 (ThermoFisher). FLIM was conducted 24 hours after transfection. For expression of FLIM markers in the DA9 neuron, each fusion protein constructs were cloned into *Asc*I and *Kpn*I sites of the pSM vector containing *mig-13* promoter using SLiCE method.

A custom-made two-photon fluorescence lifetime imaging microscope was used as described elsewhere(Murakoshi et al., 2011). Briefly, EGFP-Rap2a was excited with a Ti-sapphire laser (Mai Tai; Spectra-Physics) tuned to 920 nm. The X and Y scanning galvano mirrors (6210H; Cambridge Technology) were controlled with ScanImage software (Pologruto et al., 2003). EGFP photon signals were collected an objective lens (60×, 1.0 NA; Olympus) and a photomultiplier tube (H7422-40p; Hamamatsu) placed after a dichroic mirror (FF553-SDi01; Semrock) and emission filter (FF01-625/90; Semrock). A fluorescence lifetime curve was recorded by a time-correlated single-photon-counting board (SPC-150; Becker & Hickl) controlled with custom software. For construction of a fluorescence lifetime image, the mean

fluorescence lifetime values (τ_m) in each pixel were translated into a color-coded image. We quantified free EGFP-Rap2a and EGFP-Rap2a undergoing FRET (binding fraction) as described elsewhere (Yasuda et al., 2006). Briefly, we calculated the proportion of EGFP undergoing FRET in individual ROIs using the following formula:

$$P_{FRET} = \frac{\tau_{free}(\tau_{free} - \tau_m)}{(\tau_{free} - \tau_{FRET})(\tau_{free} + \tau_{FRET} - \tau_m)} \quad P_{FRET} = \frac{\tau_{free}(\tau_{free} - \tau_m)}{(\tau_{free} - \tau_{FRET})(\tau_{free} + \tau_{FRET} - \tau_m)} \quad \text{(Eq. 1)}$$

where τ_{free} and τ_{FRET} are the fluorescence lifetime of free EGFP and EGFP undergoing FRET, respectively.

Statistics

Prism (GraphPad) software was used for statistical analysis. one-way ANOVA was done and corrected for multiple comparisons with posthoc Tukey's multiple comparisons tests done between all genotypes. Student's t-test was used for pairwise comparison. Sample numbers were pre-determined before conducting statistical analyses.

Acknowledgements

We are grateful to Donald Moerman and his lab members for generating *rap*-3 mutant strain, providing other mutant strains, sharing reagents and for general discussions. We also thank Ryohei Yasuda for FRET sensor plasmids, Hiroshi Kawabe for human Rap2a cDNA, Richard Ikegami for *plx-2* promoter construct, Harald Hutter and Peri Kurshan for sharing strains, May Dang-Lawson and Michael Gold for unpublished biochemical experiments, Lisa Fernando for the technical support, all Mizumoto lab members and general discussions, Kang Shen, Shaul Yogev and Maulik Patel for comments on the manuscript. Some strains used in this study were

obtained from the CGC, which is funded by NIH Office of Research Infrastructure Programs (P40 OD010440) and *C. elegans* gene knock out consortium. Mizumoto Lab is funded by HFSP (CDA-00004/2014), CIHR (PJT-148667), NSERC (RGPIN-2015-04022), CFI-JELF (34722) and Tomizawa Jun-ichi and Keiko Fund for Young Scientist. KM is a recipient of Canada Research Chair and Michael Smith Foundation for Health Research Scholar.

Chen et al. Figure 1

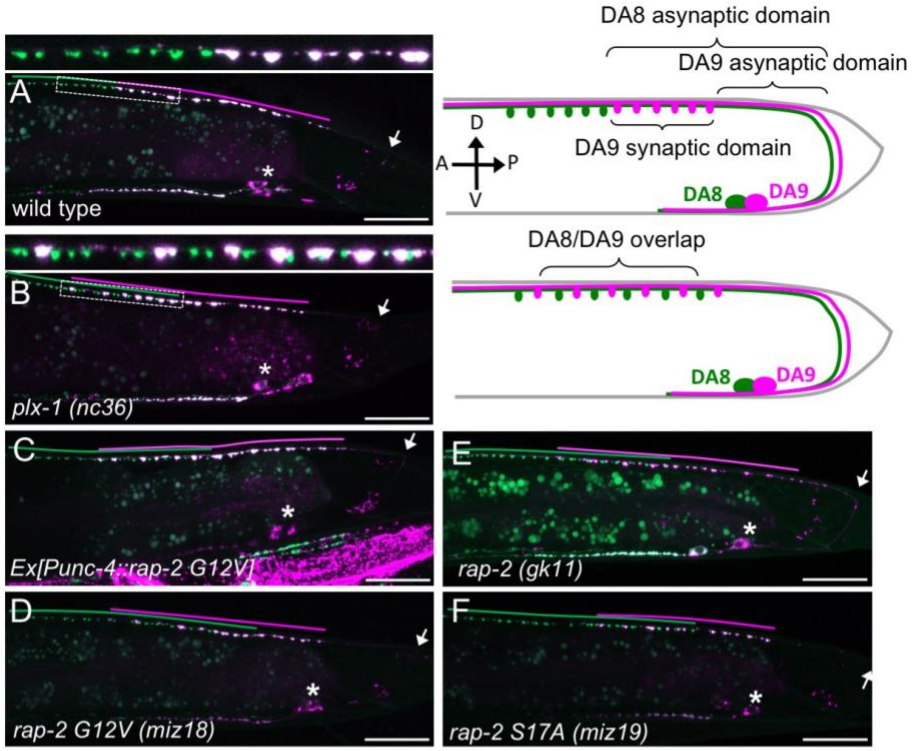

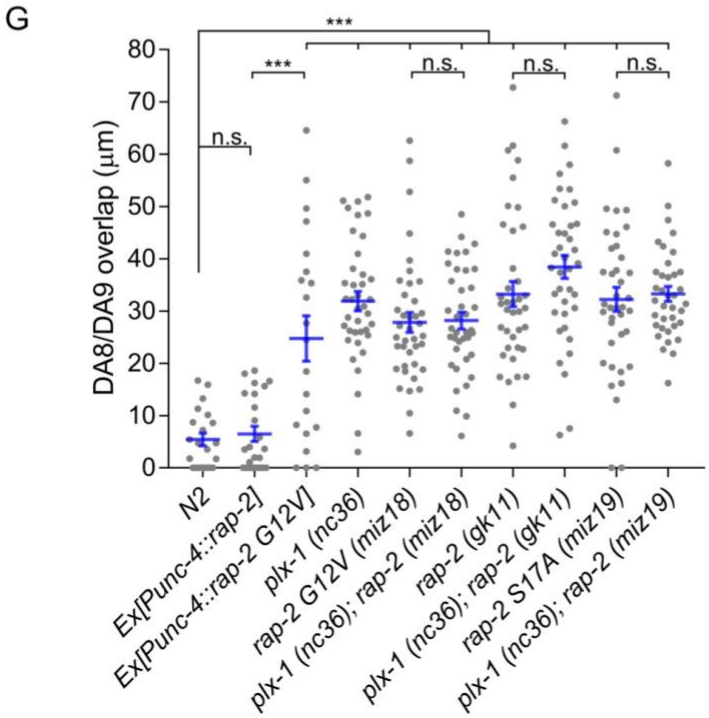

Figure 1. Gain- and loss-of-function *rap-2* mutants show synaptic tiling defects

(A and B) Representative image of synaptic tiling of wild type (A) and *plx-1* mutant (B) animals. Images show *wyIs446* marker to label synapses in DA8 (GFP::RAB-3) and DA9 (GFP::RAB-3+mCherry::RAB-3). Dotted box represents the magnified images from above of the synaptic tiling border. Schematics of DA8 (green) and DA9 (magenta) neurons with parameters for analysis shown on the right. **(C - F)** Representative images of *wyIs446* strains with the following genotypes: *rap-2(G12V)* overexpression in DA neurons (C), *rap-2 G12V (miz18)* (D), *rap-2 null (gk11)* (E) and *rap-2 S17A (miz19)* (F). Synaptic domains from DA8 and DA9 are highlighted with green and magenta lines, respectively. Asterisks: DA9 cell body. Arrows: dorsal commissure of DA9. Scale bars: 20μm. **(G)** Quantification of overlap between DA8 and DA9 synaptic domains. Each dot represents a single animal. Blue bars indicate mean ± SEM. n.s.: not significant; ***: $p < 0.001$.

Chen et al. Figure 2

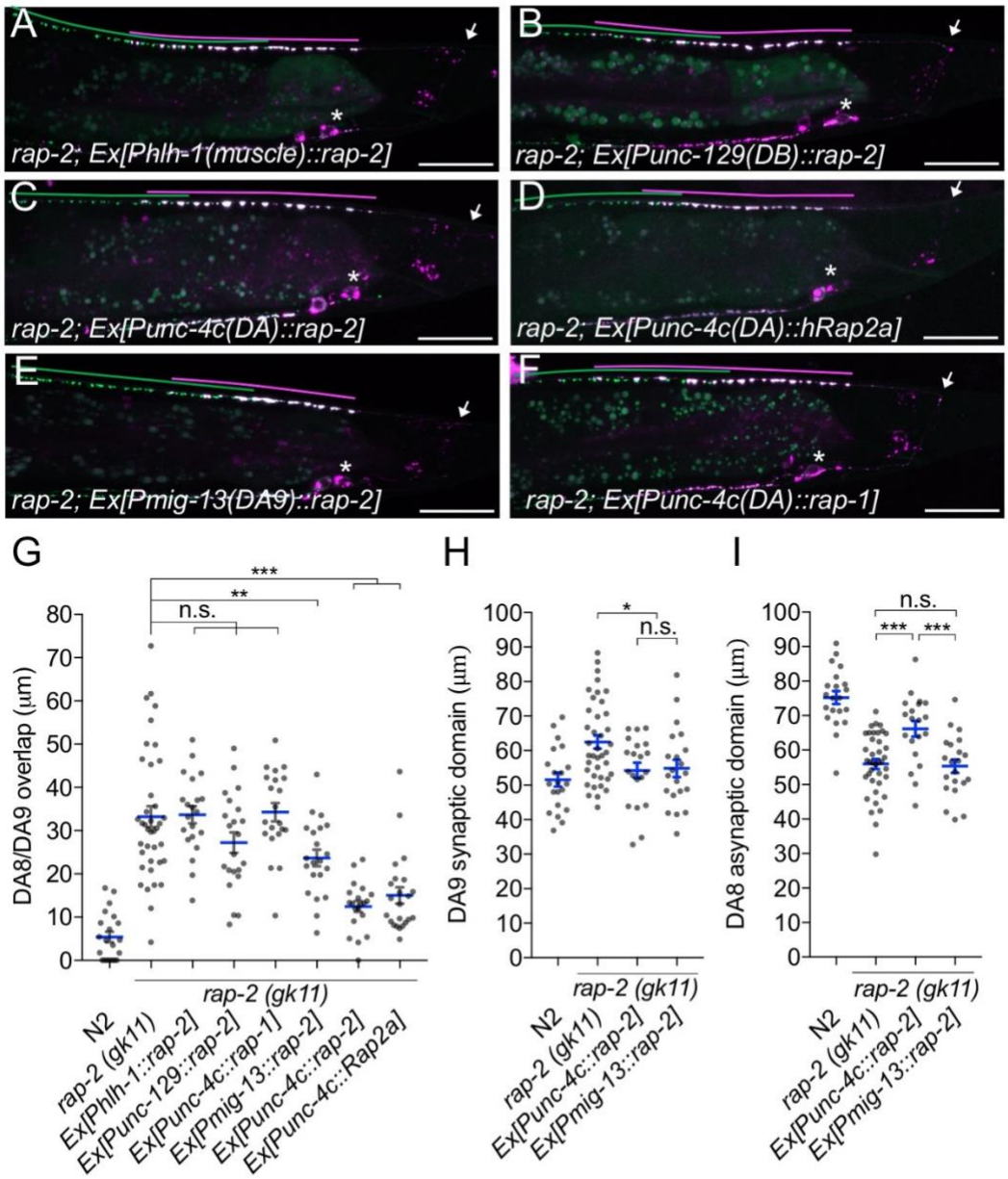

Figure 2. *rap-2* functions in DA neurons

(A - F) Representative images of *rap-2; wyIs446* animals expressing *Phlh-1::rap-2* (A), *Punc-129::rap-2* (B), *Punc-4c::rap-2* (C), *Punc-4c::Rap2a (human)* (D), *Pmig-13::rap-2* (E) and *Punc-4c;;rap-1* (F). Synaptic domains of DA8 and DA9 are highlighted with green and magenta lines, respectively. Asterisks: DA9 cell body. Arrows: dorsal commissure of DA9. Scale bars: 20µm. **(G - I)** Quantification of DA8/DA9 overlap (G), DA9 synaptic domain (H) and DA8 asynaptic domain (I). Each dot represents a single animal. Blue bars indicate mean ± SEM. n.s.: not significant; ***: $p < 0.001$; ** : $p < 0.01$; * : $p < 0.05$.

Chen et al. Figure 3

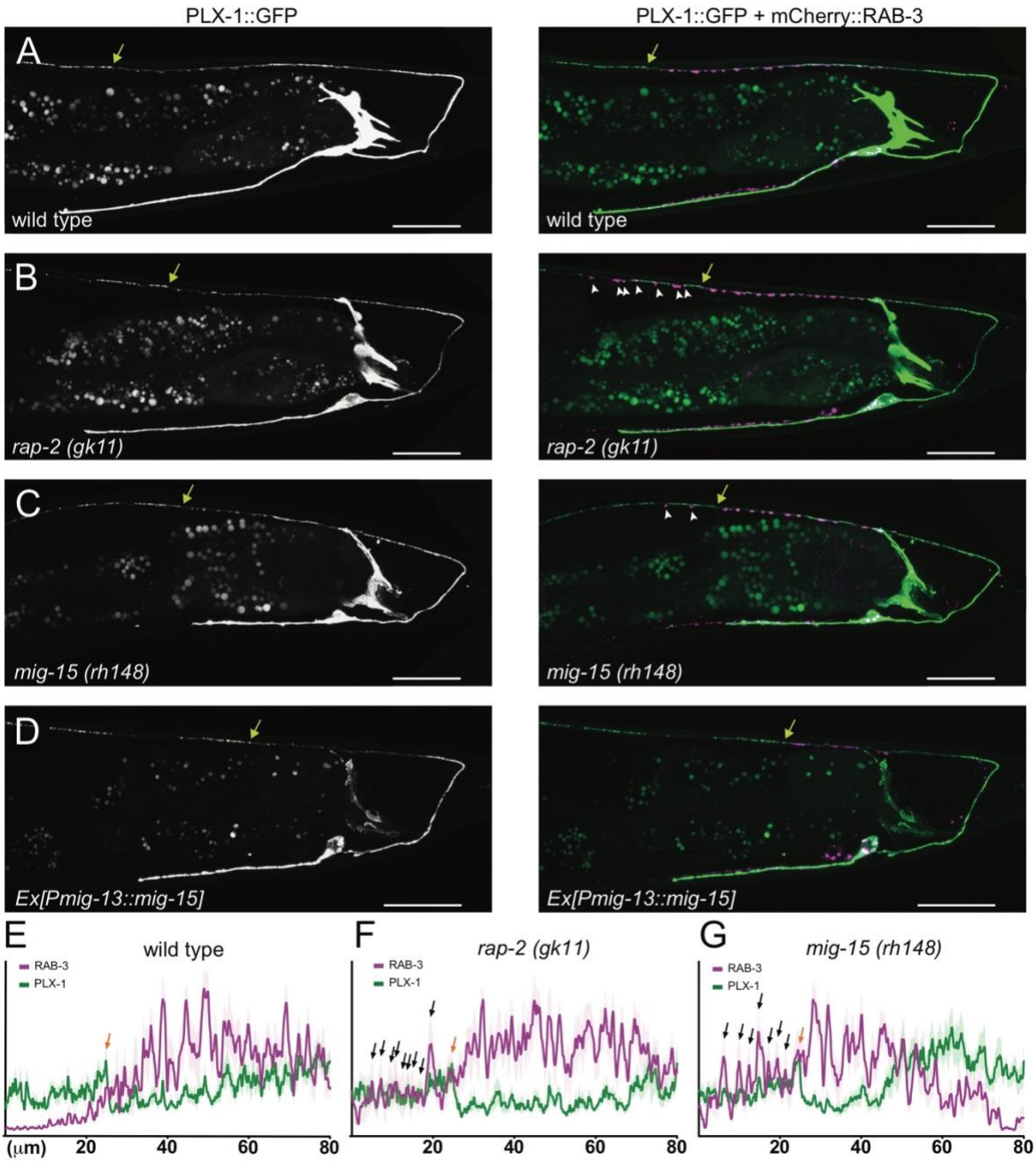

Figure 3. PLX-1::GFP localization is not affected in *rap-2* and *mig-15* mutants

(A-D) Representative image of PLX-1::GFP alone (top) and PLX-1::GFP with mCherry::RAB-3 (middle) labeled with *wyIs320* in DA9 of wildtype (**A**), *rap-2 (gk11)* (**B**) and *mig-15(rh148)* (**C**). Bracket indicates the PLX-1::GFP patch localized at the anterior edge of the DA9 synaptic domain. Arrowheads indicate ectopic synapses formed anterior to the PLX-1::GFP patch. Scale bars: 20μm. (**E-G**) Quantification of the normalized mCherry:: RAB-3 signal (magenta) and PLX-1::GFP signal (green) in the dorsal axon of DA9 in wildtype (**E**), *rap-2 (gk11)* (**F**) and *mig-15(rh148)* (**G**). Animal were aligned according to the PLX-1::GFP patch at the anterior edge of the DA9 synaptic domain (orange arrow). Light colors indicate SEM.

Chen et al. Figure 4

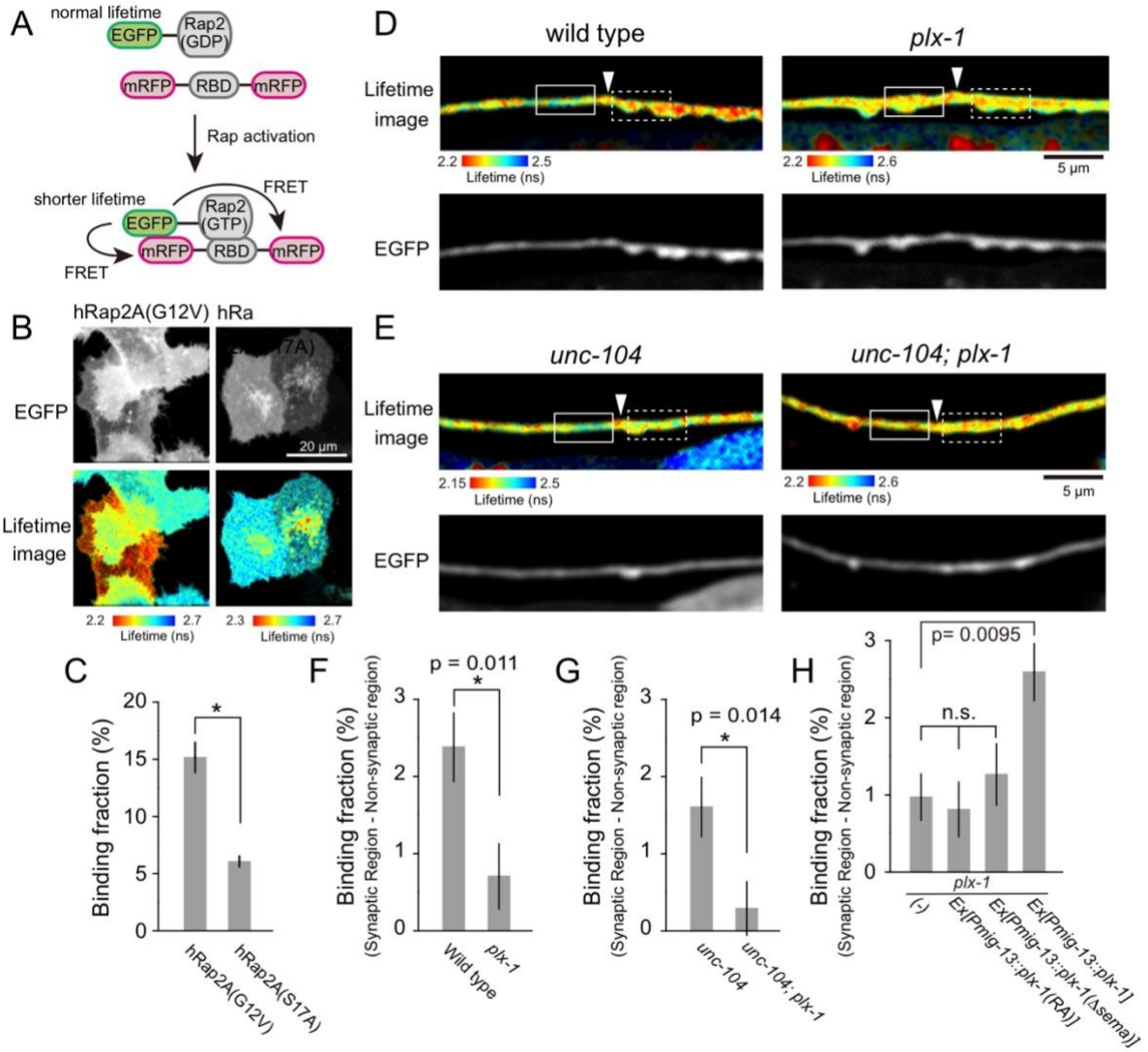

Figure 4 PLX-1 locally inhibits Rap2 activity in DA9 (A) Schematic of Rap2 FRET sensor system. Binding of mRFP- RalGDS(RBD)-mRFP to EGFP-Rap2 induces FRET from EGFP to mRFP, leading to decreased EGFP fluorescence lifetime. **(B)** Representative epifluorescence (top) and fluorescence lifetime images (bottom) of HeLa cells expressing Rap2 FRET sensor (mRFP-RalGDS(RBD)-mRFP) with either constitutively GTP(G12V)- or GDP(S17A)- forms of human Rap2a. **(C)** Quantification of the binding fraction of Rap2 mutants in HeLa cells. Binding fractions were measured from fluorescence decay curves of individual cells (G12V, n=25; S17A, n=25), as described previously (Murakoshi et al., 2011). Data are shown as mean ± SEM. Asterisks denote statistical significance ($p<0.05$, student's t-test). **(D)** Representative images of fluorescence lifetime (top) and epifluorescence (bottom) of *mizIs19* in wild type (left) and *plx-1* mutants (right). White arrowheads indicate the position of the putative synaptic tiling border, as judged by the slight dorsal shift of the DA9 axon, as reported previously (Mizumoto and Shen, 2013a). **(E)** Representative images of fluorescence lifetime (top) and epifluorescence (bottom) of *mizIs19* in *unc-104* (left) and *unc-104; plx-1* double mutants (right). **(F)** Quantification of the difference in binding fraction of GTP-Rap2a and RalGDS(RBD) between synaptic region (dotted boxes in **D**) and anterior asynaptic region (solid boxes in **D**). The binding fraction measured in synaptic region (dotted rectangle) was subtracted by that in non-synaptic region (solid rectangle). Five micrometers along the axon line from the synaptic tiling border were used for quantification. Data are presented as mean ± SEM (wild type, n=22; *plx-1*, n=17). **(G)** Quantification of the difference in binding fraction of GTP-Rap2a and RalGDS(RBD) between synaptic region (dotted boxes in **E**) and anterior asynaptic region (solid boxes in **E**). The binding fraction measured in synaptic region (dotted rectangle) was subtracted by that in non-synaptic region (solid rectangle). Five micrometers along the axon line from the synaptic tiling border were used for quantification. Data

are presented as mean ± SEM (*unc-104*, n=21; *unc-104; plx-1*, n=23). (**H**) Quantification of the difference in binding fraction of GTP-Rap2a and RalGDS(RBD) between synaptic region and anterior asynaptic region in *plx-1* mutants and *plx-1* mutants expressing rescuing constructs. Five micrometers along the axon line from the synaptic tiling border were used for quantification. Data are presented as mean ± SEM (*no array,* n=35; *Ex[Pmig-13::plx-1(RA)], n=39; Ex[Pmig-13::plx-1(Δsema)],* n=41; *Ex[Pmig-13::plx-1],* n=51).

Chen et al. Figure 5

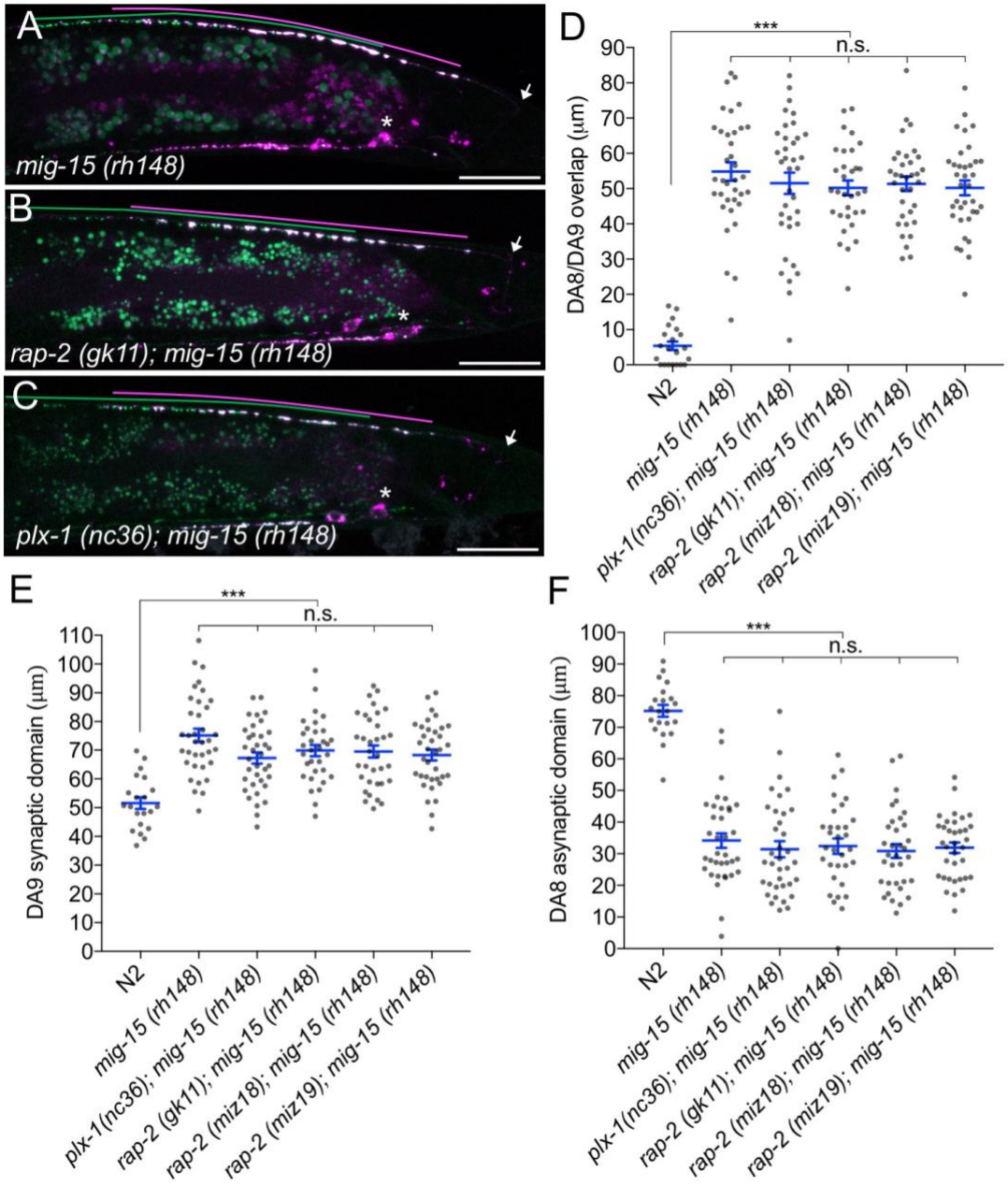

Figure 5. *mig-15(TNIK)* mutants show a severe synaptic tiling defect

(A-C) Representative images of synaptic tiling marker (*wyIs446*) in *mig-15(rh148)* (A), *rap-2(gk11); mig-15(rh148)* (B) and *plx-1(nc36); mig-15(rh148)* (C) mutants. Synaptic domains of DA8 and DA9 are highlighted with green and magenta lines, respectively. Asterisks: DA9 cell body. Arrows: dorsal commissure of DA9. Scale bars: 20μm. (**D-F**) Quantification of overlap between DA8 and DA9 synaptic domains (D), DA9 synaptic domain (E) and DA8 asynaptic domain (F) in respective mutant backgrounds. Each dot represents measurement from single animal. Blue bars indicate mean ± SEM. n.s.: not significant; *** : $p < 0.001$.

Chen et al. Figure 6

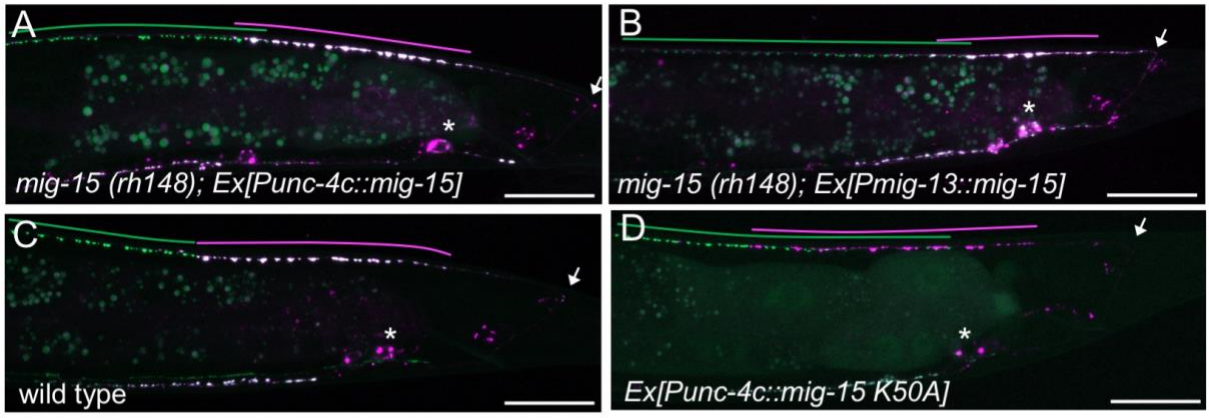

E

```
MIG-15  6 LDEIDLNSLRDPAGIFELIEVVGNGTYGQVYKGRHVKTAQLAAIKIMNINEDEEDEIKLEINMLKKHS 73
          LDEIDL++LRDPAGIFEL+E+VGNGTYGQVYKGRHVKT QLAAIK+M++  DEE+EIK EINMLKK+S
TNIK   10 LDEIDLSALRDPAGIFELVELVGNGTYGQVYKGRHVKTGQLAAIKVMDVTGDEEEEIKQEINMLKKYS 77
```

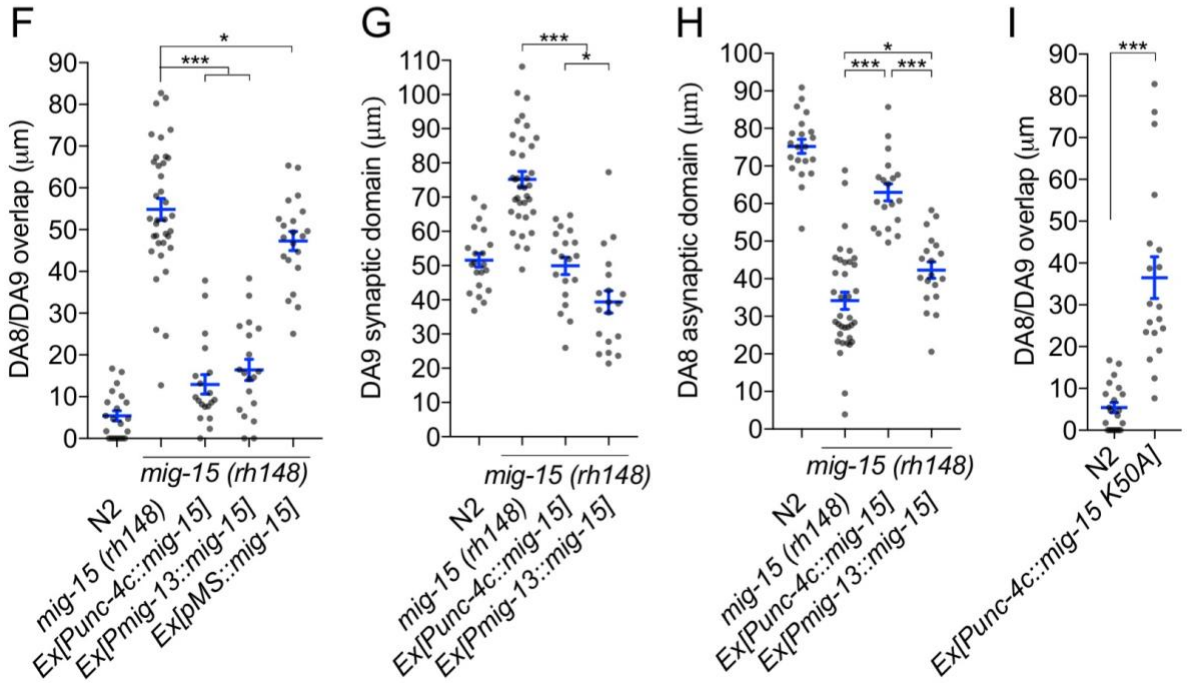

Figure 6. *mig-15* functions in DA neurons

(A-D) Representative images of synaptic tiling marker (*wyIs446*) in the following backgrounds: *mig-15(rh148); Ex[Punc-4c::mig-15]* (A), *mig-15(rh148); Ex[Pmig-13::mig-15]* (B), wild type (C) and wild type animals expressing dominant-negative *mig-15(K50A)* in DA neurons (D). Synaptic domains of DA8 and DA9 are highlighted with green and magenta lines, respectively. Asterisks: DA9 cell body. Arrows: dorsal commissure of DA9. Scale bars: 20μm. **(E)** Amino acid alignment of amino-terminal region of MIG-15 and TNIK. A kinase-dead mutation in TNIK (K54A) and corresponding mutation in MIG-15 (K50A) are highlighted in red. **(F-I)** Quantification of overlap between DA8 and DA9 synaptic domains (F and I), DA9 synaptic domain (G), DA8 asynaptic domain (H) in respective mutant backgrounds. Each dot represents measurements from a single animal. Blue bars indicate mean ± SEM. n.s.: not significant; *** : $p < 0.001$; * : $p < 0.05$.

Chen et al., Figure 7

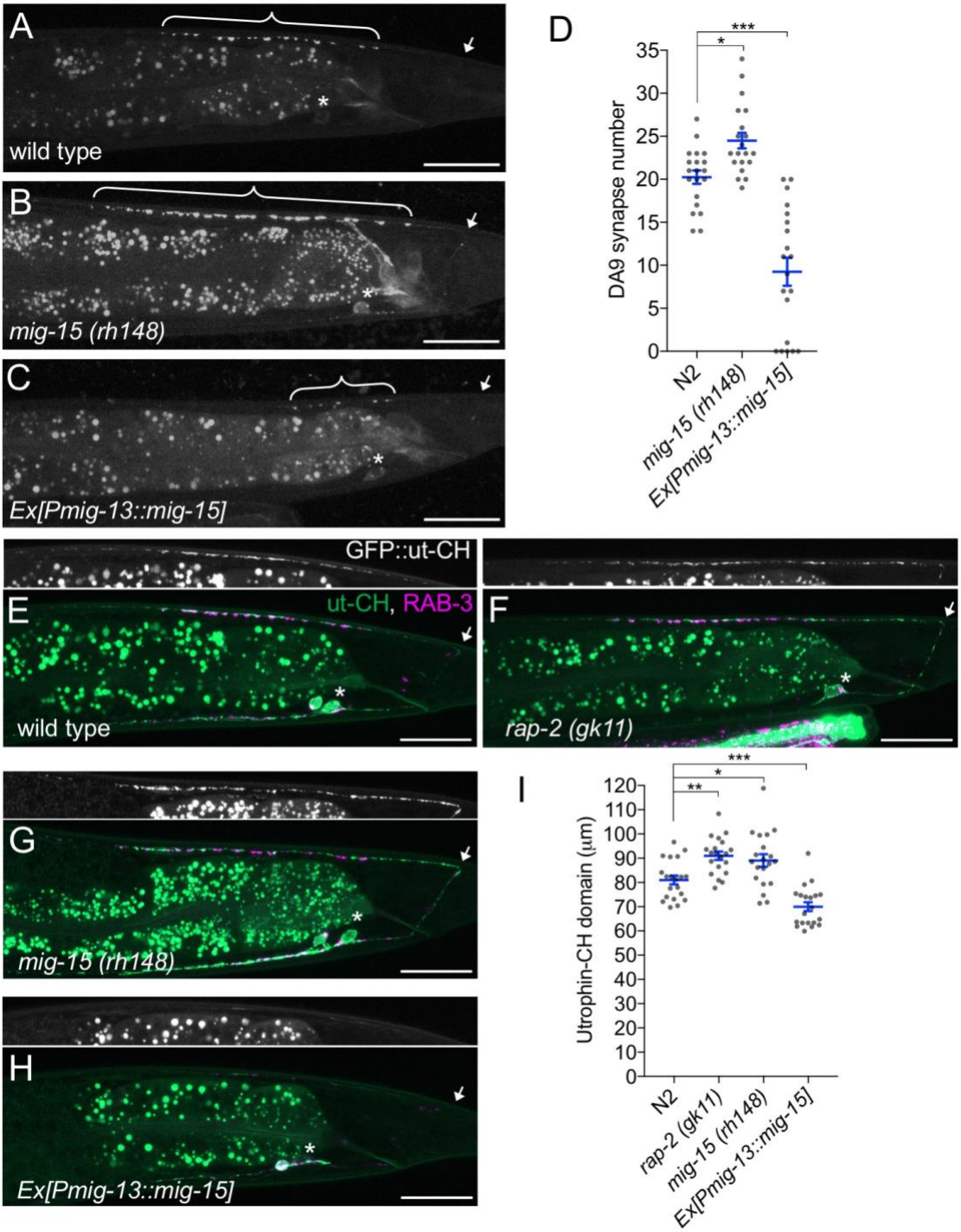

Figure 7. *mig-15* negatively regulates synapse number

(A-C) Representative images of DA9 presynaptic marker (*wyIs85*) in wild type (A), *mig-15(rh148)* (B) and *mig-15* overexpressing animals (C). Brackets represent DA9 synaptic domain. Asterisks: DA9 cell body. Arrows: dorsal commissure of DA9. Scale bars: 20µm. **(D)** Quantification of DA9 synapse number. Each dot represents measurements from a single animal. Blue bars indicate mean ± SEM. n.s.: not significant; *** : $p < 0.001$; * : $p < 0.05$. **(E-H)** Representative images of synaptic branched F-actin labeled with GFP::utCH (*wyIs329*) in wild type (E), *rap-2(gk11)* (F), *mig-15(rh148)* (G) and *mig-15* overexpressing animals (H). **(I)** Quantification of the length of GFP::utCH. Distance from the dorsal commissure to the most anterior and brightest GFP spot was measured. Blue bars indicate mean ± SEM. n.s.: not significant; ***: $p < 0.001$; **: $p<0.01$, * : $p < 0.05$.

Chen et al. Figure 8

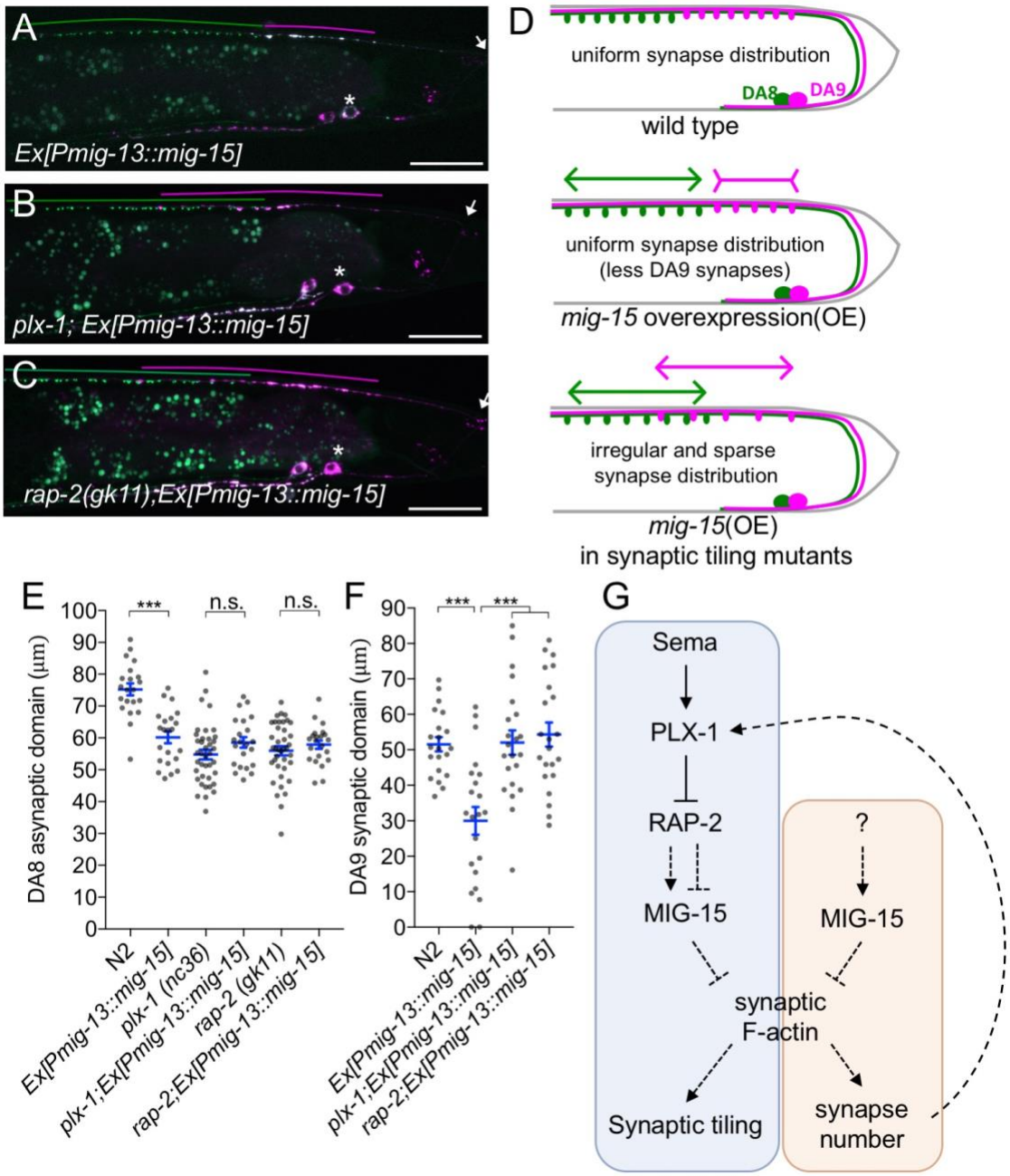

Figure 8. PLX-1/RAP-2 signaling coordinates synapse number and synaptic tiling border

(A-C) Representative images of synaptic tiling marker (*wyIs446*) overexpressing *mig-15* in DA9 from wild type (A), *plx-1(nc36)* (B) and *rap-2(gk11)* (C). Synaptic domains of DA8 and DA9 are highlighted with green and magenta lines, respectively. Asterisks: DA9 cell body. Arrows: dorsal commissure of DA9. Scale bars: 20μm. **(D)** Schematic illustration of synapse distribution in wild type (left), animals overexpressing *mig-15* in DA9 (middle) and synaptic tiling mutants overexpressing *mig-15* in DA9 (right). Arrows indicate the synaptic tiling border, and colored arrows represent expanded or shortened synaptic domain from DA8 (green) and DA9 (magenta) synaptic domains. **(E)** Quantification of the DA8 asynaptic domain. **(F)** Quantification of the DA9 synaptic domain. Each dot represents measurements from a single animal. Blue bars indicate mean ± SEM. n.s.: not significant; ***: $p < 0.001$. **(G)** A model of synaptic tiling. PLX-1/RAP-2 signaling controls synaptic tiling via MIG-15, while MIG-15 also plays crucial roles in inhibiting the number of synapses. Solid lines indicate putative direct regulations, dotted lines represent indirect or unknown mode of regulations.

References

Chapman, J.O., Li, H., Lundquist, E.A., 2008. The MIG-15 NIK kinase acts cell-autonomously in neuroblast polarization and migration in C. elegans. Dev. Biol. 324, 245–257. doi:10.1016/j.ydbio.2008.09.014

Chia, P., Patel, M., Shen, K., 2012. NAB-1 instructs synapse assembly by linking adhesion molecules and F-actin to active zone proteins. Nat. Neurosci. 15, 234–242. doi:10.1038/nn.2991

Chia, P.H., Chen, B., Li, P., Rosen, M.K., Shen, K., 2014. Local F-actin network links synapse formation and axon branching. Cell 156, 208–220. doi:10.1016/j.cell.2013.12.009

Dalpé, G., Brown, L., Culotti, J.G., 2005. Vulva morphogenesis involves attraction of plexin 1-expressing primordial vulva cells to semaphorin 1a sequentially expressed at the vulva midline. Development 132, 1387–1400. doi:10.1242/dev.01694

Dalpé, G., Zhang, L.W., Zheng, H., Culotti, J.G., 2004. Conversion of cell movement responses to Semaphorin-1 and Plexin-1 from attraction to repulsion by lowered levels of specific RAC GTPases in C. elegans. Development 131, 2073–2088. doi:10.1242/dev.01063

Duan, Y., Wang, S.-H., Song, J., Mironova, Y., Ming, G.-L., Kolodkin, A.L., Giger, R.J., 2014. Semaphorin 5A inhibits synaptogenesis in early postnatal- and adult-born hippocampal dentate granule cells. Elife 3, e04390. doi:10.7554/eLife.04390

Eastwood, S.L., Law, A.J., Everall, I.P., Harrison, P.J., 2003. The axonal chemorepellant semaphorin 3A is increased in the cerebellum in schizophrenia and may contribute to its synaptic pathology. Mol. Psychiatry 8, 148–155. doi:10.1038/sj.mp.4001233

Epstein, J.A., Aghajanian, H., Singh, M.K., 2015. Semaphorin signaling in cardiovascular development. Cell Metab. 21, 163–173. doi:10.1016/j.cmet.2014.12.015

Frische, E.W., Pellis-van Berkel, W., van Haaften, G., Cuppen, E., Plasterk, R.H.A., Tijsterman, M., Bos, J.L., Zwartkruis, F.J.T., 2007. RAP-1 and the RAL-1/exocyst pathway coordinate hypodermal cell organization in Caenorhabditis elegans. EMBO J. 26, 5083–5092. doi:10.1038/sj.emboj.7601922

Fu, Z., Lee, S.H., Simonetta, A., Hansen, J., Sheng, M., Pak, D.T.S., 2007. Differential roles of Rap1 and Rap2 small GTPases in neurite retraction and synapse elimination in hippocampal spiny neurons. J. Neurochem. 100, 118–131. doi:10.1111/j.1471-4159.2006.04195.x

Fujii, T., Nakao, F., Shibata, Y., Shioi, G., Kodama, E., Fujisawa, H., Takagi, S., 2002. Caenorhabditis elegans PlexinA, PLX-1, interacts with transmembrane semaphorins and regulates epidermal morphogenesis. Development 129, 2053–2063.

Hussain, N.K., Hsin, H., Huganir, R.L., Sheng, M., 2010. MINK and TNIK differentially act on Rap2-mediated signal transduction to regulate neuronal structure and AMPA receptor function. J. Neurosci. 30, 14786–14794. doi:10.1523/JNEUROSCI.4124-10.2010

Ikegami, R., Zheng, H., Ong, S.-H., Culotti, J., 2004. Integration of semaphorin-2A/MAB-20, ephrin-4, and UNC-129 TGF-beta signaling pathways regulates sorting of distinct sensory rays in C. elegans. Dev. Cell 6, 383–395.

Inaki, M., Yoshikawa, S., Thomas, J.B., Aburatani, H., Nose, A., 2007. Wnt4 is a local repulsive cue that determines synaptic target specificity. Curr. Biol. 17, 1574–1579. doi:10.1016/j.cub.2007.08.013

Kawabe, H., Neeb, A., Dimova, K., Young, S.M., Takeda, M., Katsurabayashi, S., Mitkovski, M., Malakhova, O.A., Zhang, D.-E., Umikawa, M., Kariya, K.-I., Goebbels, S., Nave, K.-A., Rosenmund, C., Jahn, O., Rhee, J., Brose, N., 2010. Regulation of Rap2A by the ubiquitin ligase Nedd4-1 controls neurite development. Neuron 65, 358–372. doi:10.1016/j.neuron.2010.01.007

Kolodkin, A.L., Matthes, D.J., Goodman, C.S., 1993. The semaphorin genes encode a family of transmembrane and secreted growth cone guidance molecules. Cell 75, 1389–1399.

Kolodkin, A.L., Matthes, D.J., O'Connor, T.P., Patel, N.H., Admon, A., Bentley, D., Goodman, C.S., 1992. Fasciclin IV: sequence, expression, and function during growth cone guidance in the grasshopper embryo. Neuron 9, 831–845.

Lin, K.B.L., Freeman, S.A., Gold, M.R., 2010. Rap GTPase-mediated adhesion and migration: A target for limiting the dissemination of B-cell lymphomas? Cell Adh Migr 4, 327–332. doi:10.4161/cam.4.3.11114

Lin, K.B.L., Freeman, S.A., Zabetian, S., Brugger, H., Weber, M., Lei, V., Dang-Lawson, M., Tse, K.W.K., Santamaria, R., Batista, F.D., Gold, M.R., 2008. The rap GTPases regulate B cell morphology, immune-synapse formation, and signaling by particulate B cell receptor ligands. Immunity 28, 75–87. doi:10.1016/j.immuni.2007.11.019

Liu, Z., Fujii, T., Nukazuka, A., Kurokawa, R., Suzuki, M., Fujisawa, H., Takagi, S., 2005. C. elegans PlexinA PLX-1 mediates a cell contact-dependent stop signal in vulval precursor cells. Dev. Biol. 282, 138–151. doi:10.1016/j.ydbio.2005.03.002

Mah, S., Nelson, M.R., Delisi, L.E., Reneland, R.H., Markward, N., James, M.R., Nyholt, D.R., Hayward, N., Handoko, H., Mowry, B., Kammerer, S., Braun, A., 2006. Identification of the semaphorin receptor PLXNA2 as a candidate for susceptibility to schizophrenia. Mol. Psychiatry 11, 471–478. doi:10.1038/sj.mp.4001785

Mahmoudi, T., Li, V.S.W., Ng, S.S., Taouatas, N., Vries, R.G.J., Mohammed, S., Heck, A.J., Clevers, H., 2009. The kinase TNIK is an essential activator of Wnt target genes. EMBO J. 28, 3329–3340. doi:10.1038/emboj.2009.285

Mizumoto, K., Shen, K., 2013a. Interaxonal interaction defines tiled presynaptic innervation in C. elegans. Neuron 77, 655–666. doi:10.1016/j.neuron.2012.12.031

Mizumoto, K., Shen, K., 2013b. Two Wnts instruct topographic synaptic innervation in C. elegans. Cell Rep 5, 389–396. doi:10.1016/j.celrep.2013.09.011

Nakao, F., Hudson, M.L., Suzuki, M., Peckler, Z., Kurokawa, R., Liu, Z., Gengyo-Ando, K., Nukazuka, A., Fujii, T., Suto, F., Shibata, Y., Shioi, G., Fujisawa, H., Mitani, S., Chisholm, A.D., Takagi, S., 2007. The PLEXIN PLX-2 and the ephrin EFN-4 have distinct roles in MAB-20/Semaphorin 2A signaling in Caenorhabditis elegans morphogenesis. Genetics 176, 1591–1607. doi:10.1534/genetics.106.067116

Negishi, M., Oinuma, I., Katoh, H., 2005. Plexins: axon guidance and signal transduction. Cell. Mol. Life Sci. 62, 1363–1371. doi:10.1007/s00018-005-5018-2

Neufeld, G., Shraga-Heled, N., Lange, T., Guttmann-Raviv, N., Herzog, Y., Kessler, O., 2005. Semaphorins in cancer. Front. Biosci. 10, 751–760.

Nukazuka, A., Fujisawa, H., Inada, T., Oda, Y., Takagi, S., 2008. Semaphorin controls epidermal morphogenesis by stimulating mRNA translation via eIF2alpha in Caenorhabditis elegans. Genes Dev. 22, 1025–1036. doi:10.1101/gad.1644008

Nukazuka, A., Tamaki, S., Matsumoto, K., Oda, Y., Fujisawa, H., Takagi, S., 2011. A shift of the TOR adaptor from Rictor towards Raptor by semaphorin in C. elegans. Nat Commun 2, 484. doi:10.1038/ncomms1495

O'Connor, T.P., Cockburn, K., Wang, W., Tapia, L., Currie, E., Bamji, S.X., 2009. Semaphorin 5B mediates synapse elimination in hippocampal neurons. Neural Dev 4, 18. doi:10.1186/1749-8104-4-18

Ohba, Y., Mochizuki, N., Matsuo, K., Yamashita, S., Nakaya, M., Hashimoto, Y., Hamaguchi, M., Kurata, T., Nagashima, K., Matsuda, M., 2000. Rap2 as a slowly responding molecular switch in the Rap1 signaling cascade. Mol. Cell. Biol. 20, 6074–6083.

Pecho-Vrieseling, E., Sigrist, M., Yoshida, Y., Jessell, T.M., Arber, S., 2009. Specificity of sensory-motor connections encoded by Sema3e-Plxnd1 recognition. Nature 459, 842–846. doi:10.1038/nature08000

Pellis-van Berkel, W., Verheijen, M.H.G., Cuppen, E., Asahina, M., de Rooij, J., Jansen, G., Plasterk, R.H.A., Bos, J.L., Zwartkruis, F.J.T., 2005. Requirement of the Caenorhabditis elegans RapGEF pxf-1 and rap-1 for epithelial integrity. Mol. Biol. Cell 16, 106–116. doi:10.1091/mbc.E04-06-0492

Poinat, P., De Arcangelis, A., Sookhareea, S., Zhu, X., Hedgecock, E.M., Labouesse, M., Georges-Labouesse, E., 2002. A conserved interaction between beta1 integrin/PAT-3 and Nck-interacting kinase/MIG-15 that mediates commissural axon navigation in C. elegans. Curr. Biol. 12, 622–631.

Shakir, M.A., Gill, J.S., Lundquist, E.A., 2006. Interactions of UNC-34 Enabled with Rac GTPases and the NIK kinase MIG-15 in Caenorhabditis elegans axon pathfinding and neuronal migration. Genetics 172, 893–913. doi:10.1534/genetics.105.046359

Schmitz, C., Wacker, I., Hutter, H., 2008. The Fat-like cadherin CDH-4 controls axon fasciculation, cell migration and hypodermis and pharynx development in Caenorhabditis elegans. Dev. Biol. 316(2):249-259

Shen, K., Bargmann, C.I., 2003. The immunoglobulin superfamily protein SYG-1 determines the location of specific synapses in C. elegans. Cell 112, 619–630.

Shen, K., Fetter, R.D., Bargmann, C.I., 2004. Synaptic specificity is generated by the synaptic guidepost protein SYG-2 and its receptor, SYG-1. Cell 116, 869–881.

Taira, K., Umikawa, M., Takei, K., Myagmar, B.-E., Shinzato, M., Machida, N., Uezato, H., Nonaka, S., Kariya, K.-I., 2004. The Traf2- and Nck-interacting kinase as a putative effector of Rap2 to regulate actin cytoskeleton. J. Biol. Chem. 279, 49488–49496. doi:10.1074/jbc.M406370200

Takamatsu, H., Kumanogoh, A., 2012. Diverse roles for semaphorin-plexin signaling in the immune system. Trends Immunol. 33, 127–135. doi:10.1016/j.it.2012.01.008

Teulière, J., Gally, C., Garriga, G., Labouesse, M., Georges-Labouesse, E., 2011. MIG-15 and ERM-1 promote growth cone directional migration in parallel to UNC-116 and WVE-1. Development 138, 4475–4485. doi:10.1242/dev.061952

Tran, T.S., Kolodkin, A.L., Bharadwaj, R., 2007. Semaphorin regulation of cellular morphology. Annu. Rev. Cell Dev. Biol. 23, 263–292. doi:10.1146/annurev.cellbio.22.010605.093554

Tran, T.S., Rubio, M.E., Clem, R.L., Johnson, D., Case, L., Tessier-Lavigne, M., Huganir, R.L., Ginty, D.D., Kolodkin, A.L., 2009. Secreted semaphorins control spine distribution and morphogenesis in the postnatal CNS. Nature 462, 1065–1069. doi:10.1038/nature08628

Wang, Y., He, H., Srivastava, N., Vikarunnessa, S., Chen, Y.-B., Jiang, J., Cowan, C.W., Zhang, X., 2012. Plexins are GTPase-activating proteins for Rap and are activated by induced dimerization. Sci Signal 5, ra6–ra6. doi:10.1126/scisignal.2002636

Wang, Y., Pascoe, H.G., Brautigam, C.A., He, H., Zhang, X., 2013. Structural basis for activation and non-canonical catalysis of the Rap GTPase activating protein domain of plexin. Elife 2, e01279. doi:10.7554/eLife.01279

White, J.G., Southgate, E., Thomson, J.N., Brenner, S., 1986. The structure of the nervous system of the nematode Caenorhabditis elegans. Philos. Trans. R. Soc. Lond., B, Biol. Sci. 314, 1–340.

Zhu, J.J., Qin, Y., Zhao, M., van Aelst, L., Malinow, R., 2002. Ras and Rap control AMPA receptor trafficking during synaptic plasticity. Cell 110, 443–455.

Zhu, Y., Pak, D., Qin, Y., McCormack, S.G., Kim, M.J., Baumgart, J.P., Velamoor, V., Auberson, Y.P., Osten, P., van Aelst, L., Sheng, M., Zhu, J.J., 2005. Rap2-JNK removes synaptic AMPA receptors during depotentiation. Neuron 46, 905–916. doi:10.1016/j.neuron.2005.04.037

Supplemental information

Chen et al. Supplemental Figure 1

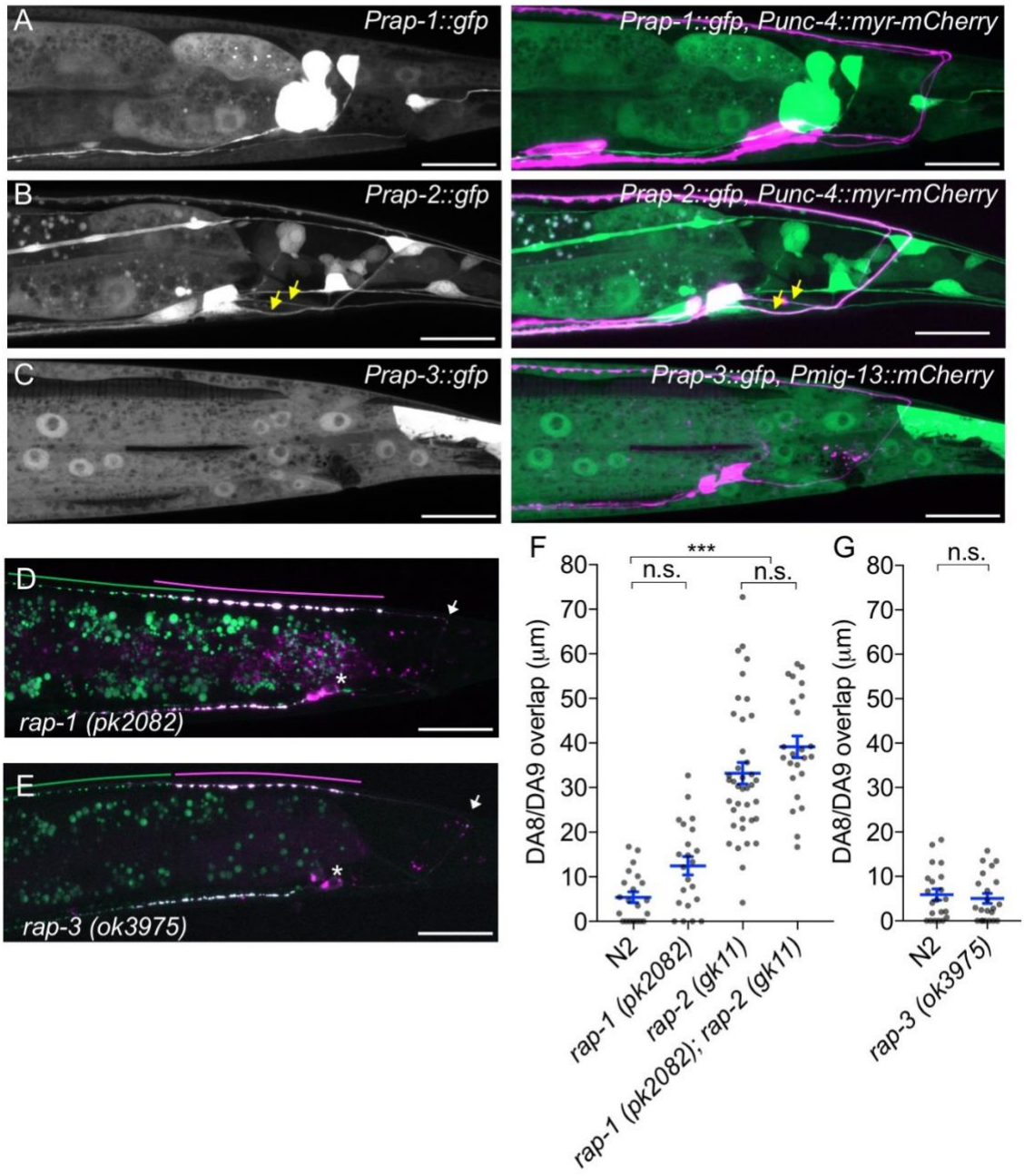

Supplemental Figure 1. *rap-1* and *rap-3* are not involved in synaptic tiling of DA8 and DA9

(A-C) Representative images of P*rap-1::GFP* (*wyEx5445*) (A), P*rap-2::GFP* (*wyEx5464*) (B) and P*rap-3::GFP* (*mizEx194*) (C). Merged images with DA markers are shown on the right. **(D)** Representative image of synaptic tiling marker (*wyIs446*) in *rap-1* mutants. **(E)** Representative image of synaptic tiling marker (*wyIs524*) in *rap-3* mutants. *wyIs524* was used due to the linkage between *wyIs446* and *rap-3*. Synaptic domains of DA8 and DA9 are highlighted with green and magenta lines, respectively. Asterisks: DA9 cell body. Arrows: dorsal commissure of DA9. Scale bars: 20μm. **(F and G)** Quantification of DA8/DA9 overlap. Blue bars indicate mean ± SEM. n.s.: not significant; ***: $p < 0.001$.

Chen et al. Supplemental Figure 2

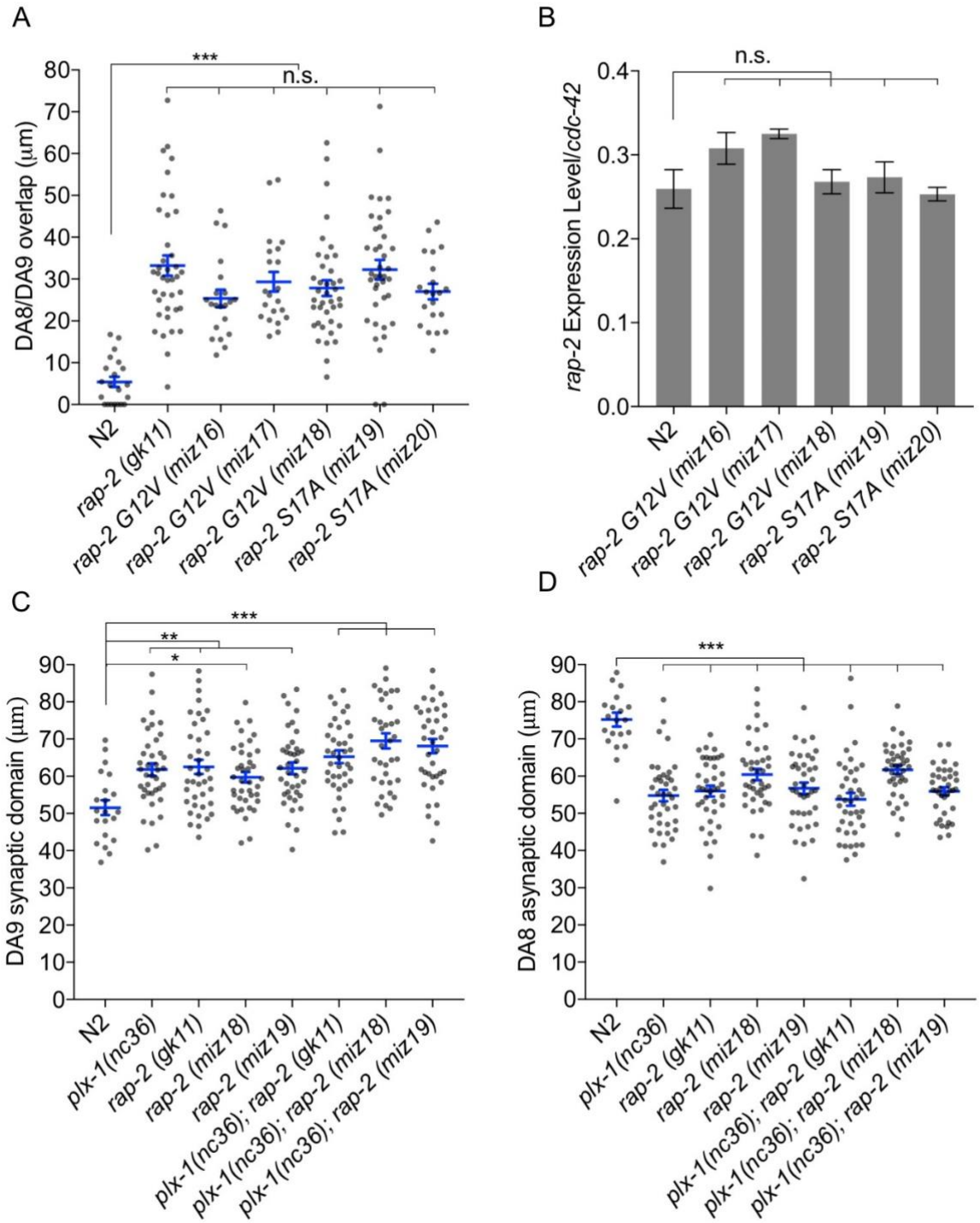

Supplemental Figure 2. Both GTP- and GDP-bound forms of RAP-2 are required for synaptic tiling. (A) Quantification of DA8/DA9 overlap. Blue bars indicate mean ± SEM. n.s.: not significant; ** : $p < 0.001$. **(B)** RT-qPCR analysis of *rap-2* CRISPR mutants. *cdc-42* was used as an internal reference. Average of 3 independent qPCR reactions are shown. Bars indicate mean ± SEM. n.s.: not significant. (C) Quantification of DA9 synaptic domain length. (D) Quantification of DA8 asynaptic domain length. Blue bars indicate mean ± SEM. n.s.: not significant; ***: $p < 0.001$; **: $p<0.01$, * : $p < 0.05$.

Chen et al. Supplemental Figure 3

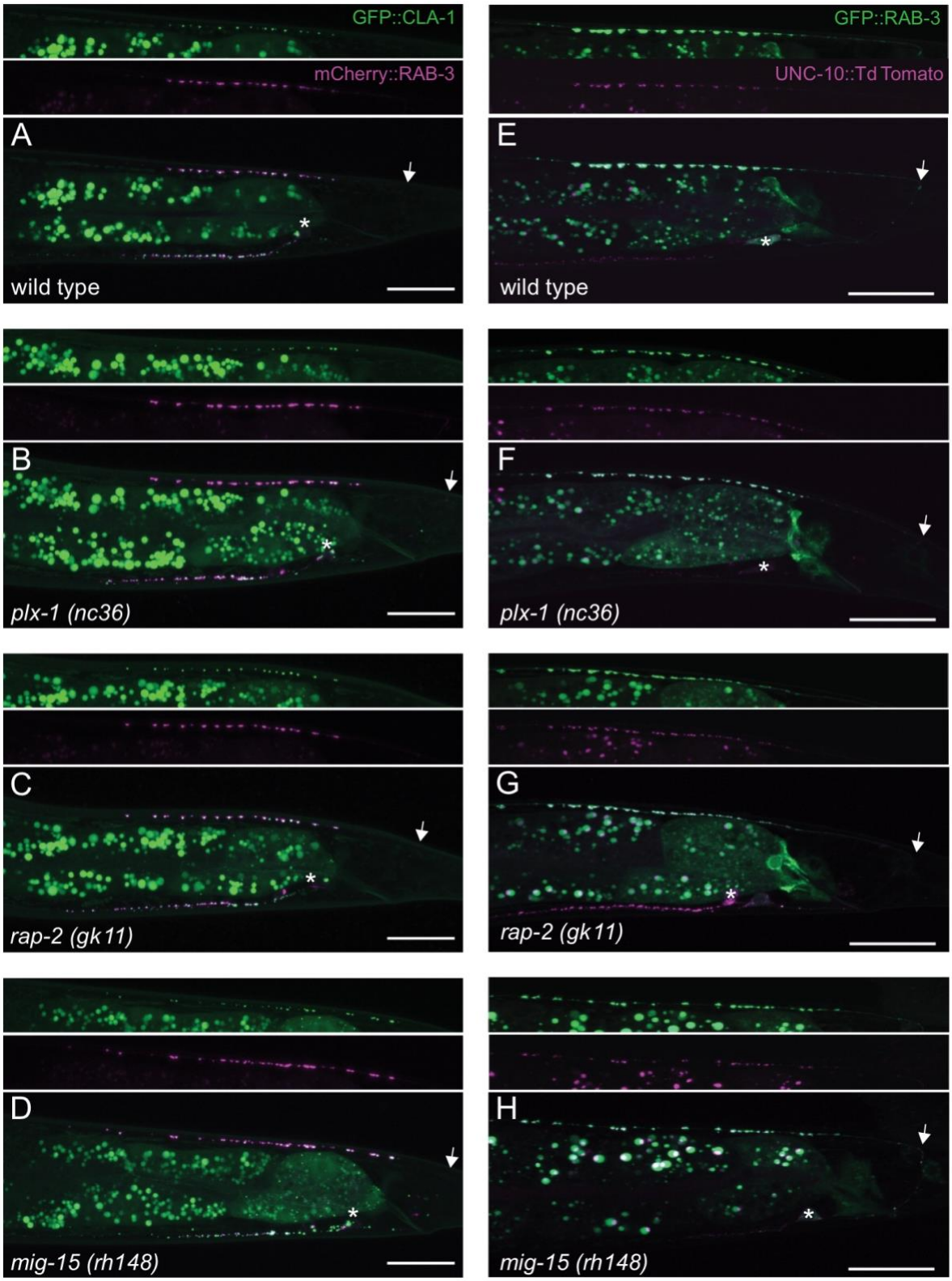

Supplemental Figure 3 Co-localization between RAB-3 and the active zone marker, CLA-1.

(A-D) Representative images of DA9 synaptic vesicle marker, mCherry::RAB-3, and active zone marker, CLA-1::3xGFPnovo2 (*wyIs685*) in wild type (A), *plx-1* (B), *rap-2* (C) and *mig-15* (D). **(E-H)** Representative images of DA9 synaptic vesicle marker, GFP::RAB-3(*wyIs85*), and active zone marker, UNC-10::TdTomato (*mizEx272*) in wild type (E), *plx-1* (F), *rap-2* (G) and *mig-15* (H). Arrows represent the position of DA9 commissure. Asterisks indicate DA9 cell body. Scale bars: 20μm.

Chen et al. Supplemental Figure 4

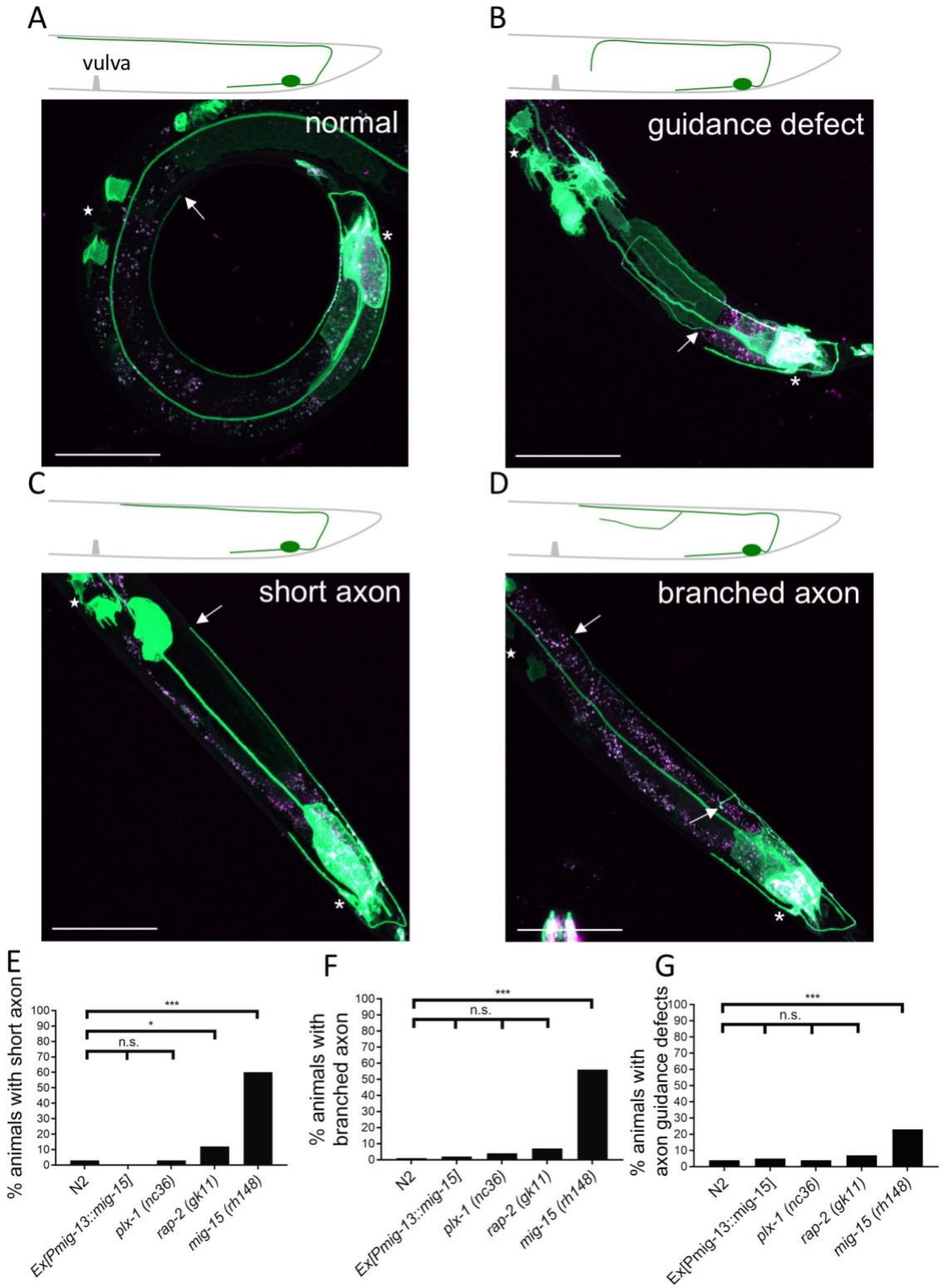

Supplemental Figure 4. Morphological defects of DA9 axon in *mig-15(rh148)* mutants. (A-D) Representative images of DA9 marker (*mizIs1*) in *mig-15(rh148)* mutants with normal structure (A), axon guidance defect (B), short axon (C) and branched axon (D). Scale bars: 50μm. Stars indicate the position of vulva. Asterisks: DA9 cell body. Arrows: position of DA9 axonal tip. In wild type, DA9 axon extends beyond the vulva. We defined a short axon as not reaching the vulva. **(E-G)** Quantification of DA9 axonal defects represented in B-D in each genetic background (n=100). n.s.: not significant; ***: $p < 0.001$; *: $p < 0.05$.

Chen et al. Supplemental Figure 5

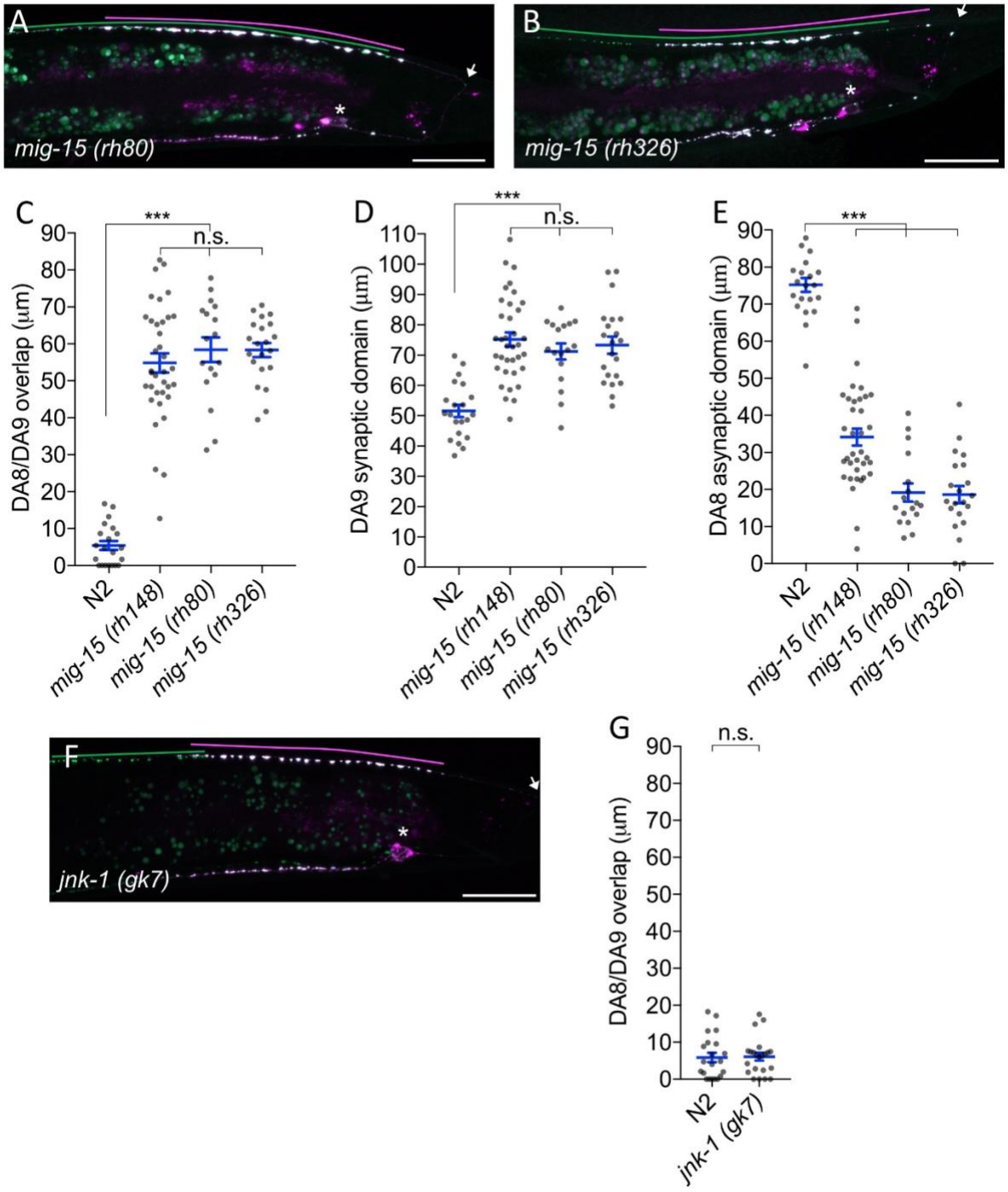

Supplemental Figure 5. Synaptic tiling defect in *mig-15* mutants

(A and B) Representative images of synaptic tiling marker (*wyIs446*) in *mig-15(rh80)* (A) and *mig-15(rh326)* (B) mutants. Synaptic domains of DA8 and DA9 are highlighted with green and magenta lines, respectively. Asterisks: DA9 cell body. Arrows: dorsal commissure of DA9. Scale bars: 20μm. **(C-E)** Quantification of DA8/DA9 overlap (C), DA9 synaptic domain (D) and DA8 asynaptic domain (E). Each dot represents measurement from single animal. Blue bars indicate mean ± SEM. n.s.: not significant; ***: $p < 0.001$. **(F)** Representative image of synaptic tiling marker (*wyIs524*) in *jnk-1* mutants. Synaptic domains of DA8 and DA9 are highlighted with green and magenta lines, respectively. Asterisks: DA9 cell body. Arrows: dorsal commissure of DA9. Scale bars: 20μm. **(G)** Quantification of DA8/DA9 overlap. Each dot represents measurements from a single animal. Blue bars indicate mean ± SEM. n.s.: not significant.

Chen et al. Supplemental Figure 6

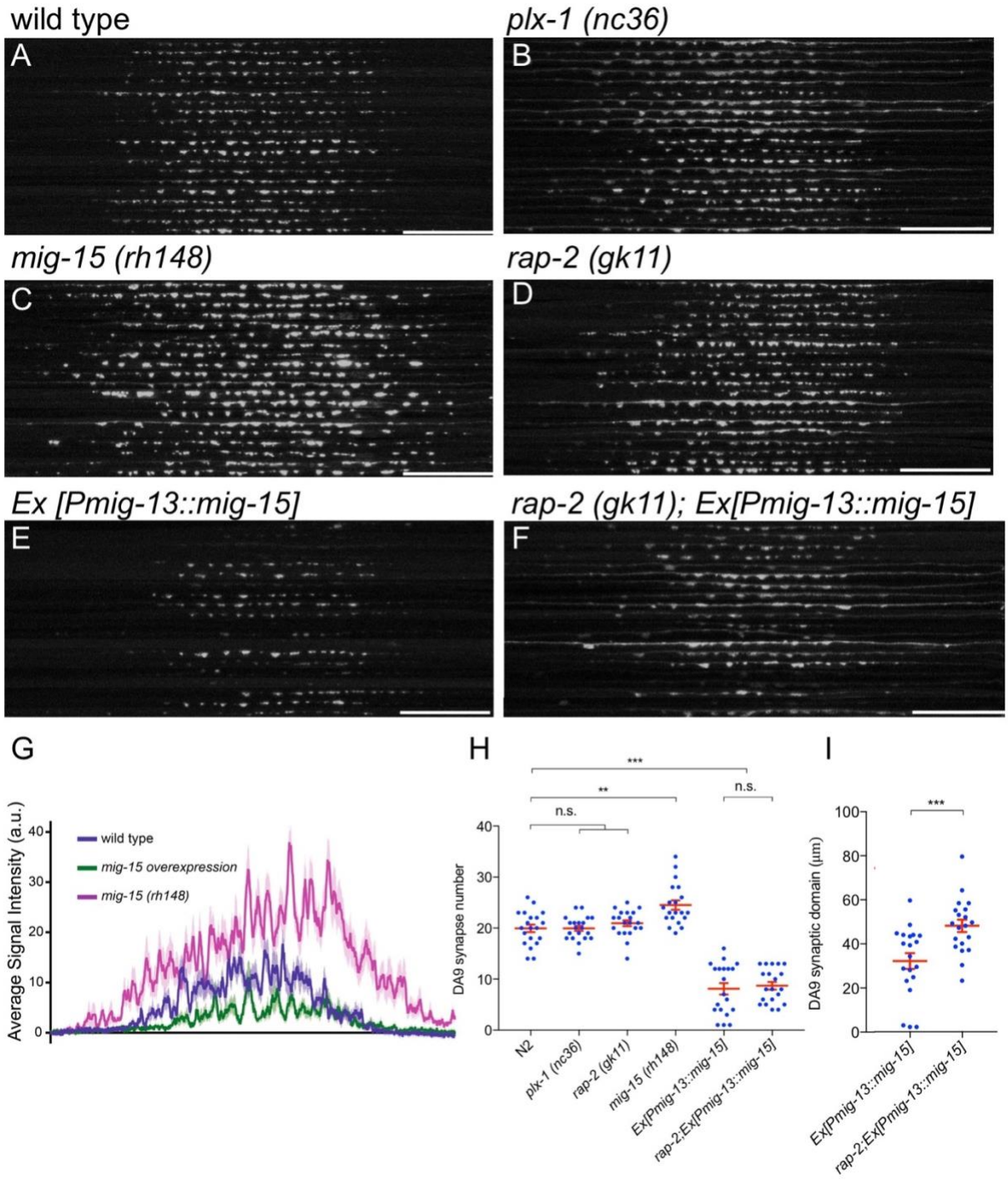

Supplemental Figure 6. *mig-15* is a negative regulator of synapse formation

(A-F) 20 confocal images of DA9 synapses (*wyIs85*) in wild type (A), *plx-1(nc36)* (B), *mig-15(rh148)* (C), *rap-2(gk11)* (D), *mizEx151 (mig-15(OE))* (E) and *rap-2(gk11); mizEx151* (F). Dorsal axon from the commissure (right end of each image) of DA9 was straightened and aligned along the anterior-posterior axis. Scale bars: 20μm. (**G**) Quantification of the signal intensity of GFP::RAB-3 in panels A to C. (**H**) Quantification of the synapse numbers in panels A to F. Each dot represents measurement from single animal. Red bars indicate mean ± SEM. n.s.: not significant; **: $p<0.01$; ***: $p < 0.001$. (I) Quantification of the DA9 synaptic domain length in panels E and F. Each dot represents measurement from single animal. Red bars indicate mean ± SEM. ***: $p < 0.001$.

Chen et al. Supplemental Figure 7

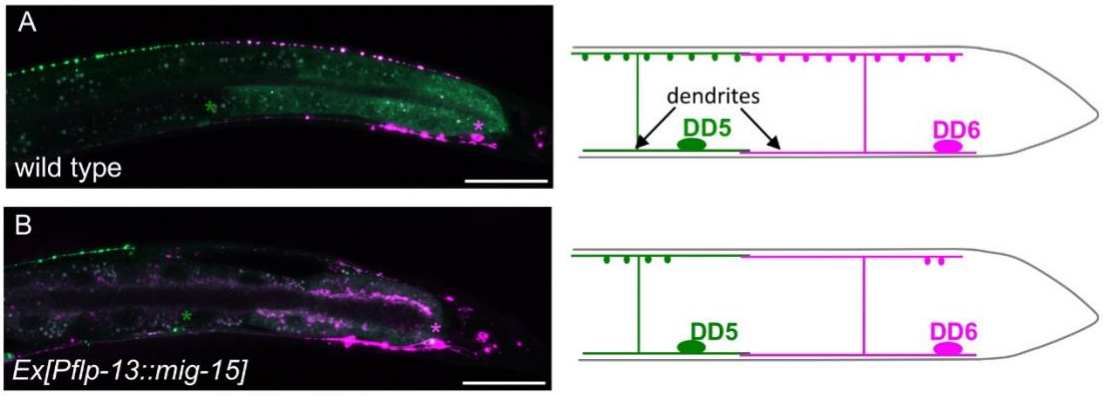

Supplemental Figure 7. Overexpression of *mig-15* reduces synapse numbers in GABAergic motor neurons

Synapses of DD5 (GFP::RAB-3) and DD6 (GFP::RAB-3+mCherry::RAB-3) (*wyIs442*) in wild type (A) and animals overexpressing *mig-15* in DD neurons (B). Schematics of the DD5 (green) and DD6 (magenta) neurons are shown in the right. Green and magenta asterisks represent the position of DD5 and DD6 cell bodies, respectively. Scale bars: 20μm.

Chen et al. Supplemental Figure 8

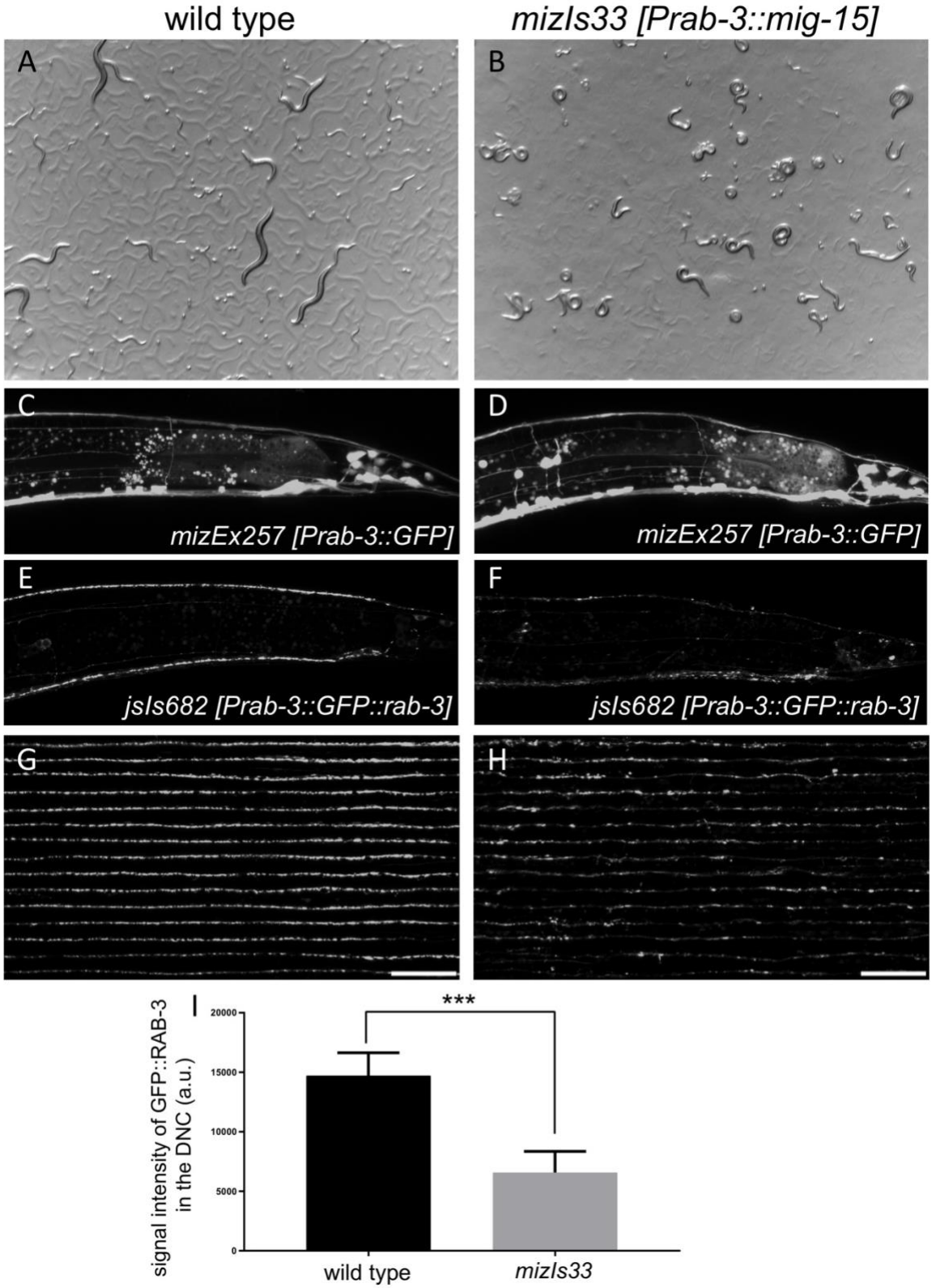

Supplemental Figure 8. Reduction of synapses by *mig-15* overexpression caused severe locomotion defects

(**A** and **B**) Stereoscopic images of wild type (A) and *mizIs33 (Prab-3::mig-15)* (B). Note that wildtype animals show normal sinusoidal body bending pattern, while *mig-15* overexpressing animals are severely uncoordinated. (**C** and **D**) Axonal morphology labeled with *mizEx257 (Prab-3::GFP)* in wild type (C) and *mivzIs33* (D). (**E** and **F**) Synapse distribution labeled with *jsIs682 (Prab-3::GFP::rab-3)* in wild type (E) and *mizIs33* (F). Synapses in the dorsal nerve cord were severely reduced. (**G** and **H**) 15 confocal images of synapses in the dorsal nerve cord (*jsIs682*) in wild type (G) and *mizIs33 (mig-15 overexpression)* (H). Middle part of the dorsal nerve cord was straightened and aligned along the anterior-posterior axis. Scale bars: 20μm. (**I**) Quantification of the total signal intensity of GFP::RAB-3 in the dorsal nerve cord shown in G and H. 155μm region of the middle part of the dorsal nerve cord was used for quantification. Data are presented as mean ± SEM (n = 15). ***: $p < 0.001$ (student's t-test).

Supplemental Experimental Procedures

RT-qPCR

Total RNA was prepared from the mixed stage of wild type and *rap-2* CRISPR mutants animals using GeneJET RNA purification kit (Thermo Fisher Scientific). RT-qPCR was conducted using Luna® Universal One-Step RT-qPCR Kit (NEB) and CFX384 Touch™ Real-Time PCR Detection System (Bio-Rad) according to the manufacturer's instructions. *cdc-42* was used as an internal reference.

List of primers

genotyping

plx-1(nc36):
Forward: CTTCGAGAGCCCCCTCATTCTTGATG
Reverse: CCGGCACACGTTAAACTAGTGCTACCG

rap-2(gk11):
Forward TCTCATCTCCATCGTCGTTCCTGC;
wild type Reverse GAGGGAGTTCAAAGTGGTCGTTC;
mutant Reverse TCCATTCACTGAATGTTCCGC

rap-2(miz16) PCR products from *miz16* allele can be digested with *Bam*HI.
Forward: TGATTTTTCGACCGTTGTGGCTC
Reverse: GCCGAAAAACACATAGAATCCCC

rap-2(miz17 - 20)
wildtype Forward: AAGTGGTCGTTCTGGGTAGT
mutant Forward: AAGTCGTGGTTCTTGGTTCA
Reverse: GGCTCGAATTTACCAGATTTTACG

rap-3 (gk3975):
Forward: CTTGTTAACTTCAGGTTCCACTGGG
Reverse: GTTCTGGTTGAGCCTTGCACTAGTC

jnk-1 (gk7)
Forward: TATCGAGTCCGTTGGGAATGTGAG
wild type Reverse: GTTCCATGAGAATTCCTCCTCCTG
mutant Reverse: GCCCGATAGTATCTTGTCACAACG

plasmid construction

rap-1 promoter (cloned into *Sph*I/*Asc*I sites of the pSM vector)
Forward: GGGCATGCCAATTCTCAATCATTAGTTTTCGGG
Reverse: GGGGCGCGCCTCTTTTTTTGAAGATCTGTTATGGTGT

rap-2 promoter (cloned into *Sph*I/*Asc*I sites of the pSM vector)
Forward: GGGGCATGCGTGTGATCTCCGGAGCAATTTG
Reverse: GGGGGCGCGCCTGAGAGTTTTTTGCTGAAAATC

rap-3 promoter (cloned into *Sph*I/*Asc*I sites of the pSM vector)
Forward: GGGGCATGCCGCTCTAGTACCATCTTTCC
Reverse: GGGGGCGCGCCCTCTTTCATTTCTTTTTGTATC

rap-1 cDNA (cloned into *Asc*I/*Kpn*I sites of the ΔpSM vector)
Forward: GGGGGCGCGCCATGCGGGAGTATAAGATTGTTGTGC
Reverse: GGGGGTACCTCACATGATGACACACGAGCAGCACTG

rap-2 cDNA (cloned into *Asc*I/*Kpn*I sites of the ΔpSM vector)
Forward: GGGGGCGCGCCATGAGGGAGTTCAAAGTGGTCG
Reverse: GGGGGTACCTCACATCAGAGAGCAACATGATTTG

rap-2 G12V mutation
Forward: TTCTGGGTAGTGTTGGTGTCGGAAAA
Reverse: TTTTCCGACACCAACACTACCCAGAA

rap-2 S17A mutation
Forward: GGTGTCGGAAAAGCCGCGTTGACGGTGCA
Reverse: TGCACCGTCAACGCGGCTTTTCCGACACC

rap-2 repair template (cloned into *Eco*RI site of the pBluescriptII SK+ vector)
Forward: CGATAAGCTTGATATCGAAAGCTACGATCGCTCGTGTAC
Reverse: GATCCCCCGGGCTGCAGGAACGGCCAATTTGTCCCATTCC

mig-15 genomic DNA (cloned into *Asc*I/*Kpn*I sites of the ΔpSM vector)
Forward: GGGGGCGCGCCATGTCGTCATCAGGACTCGACGAGATTGA
Reverse: GGGGGTACCTTACCAATTTGTCAACCCTGGCTTATTTA

hRap2a cDNA (cloned into *Asc*I/*Kpn*I sites of the pSM vector)
Forward: GGGGGCGCGCCATGCGCGAGTACAAAGTGGTGGTG
Reverse: GGGGGTACCCTATTGTATGTTACATGCAGAACAG

human Rap2a cDNA (cloned into *Xho*I/*Bam*HI sites of pCI-eGFP-Rap1 plasmid to replace Rap1 with Rap2a)
wildtype Forward: GATCTCGAGGGATGCGCGAGTACAAAGTGGTGGTGCTGGGCTC
G12V Forward:
ATCTCGAGGGATGCGCGAGTACAAAGTGGTGGTGCTGGGCTCGGTCGGGG

S17A Forward:
ATCTCGAGGGATGCGCGAGTACAAAGTGGTGGTGCTGGGCTCGGGCGGGGTAGGCA
AAGCCG
Reverse: GGTGGATCCACCTCCGGAGCCTTTGTCAGGCTG

eGFP-Rap2a (cloned into *Asc*I/*Kpn*I sites of the ΔpSM vector with *mig-13* promoter)
Forward: ATTCAGAATTTCAGGTAGGCGCGCCATGGTGAGCAAGGGCGAGGA
Reverse: CTCAGATATCAATACCATGGTACCCTATTGTATGTTACATGCAGAAC

CRISPR
rap-2 sgRNA
Forward: GTCGGAAAATGTTTTAGAGCTAGAAATAGCAAG
Reverse: ACCTCCACTACAAACATTTAGATTTGCAATTCAATTATATAG

rap-2 repair template (cloned into *Eco*RI site of the pBluescriptII SK+ vector)
5' fragment and 3'fragment were amplified separately and cloned simultaneously into the pBluescript SK(+) using SLiCE method.
5' Forward: CGATAAGCTTGATATCGAAAGCTACGATCGCTCGTGTAC
5' Reverse: CTGAACCAAGAACCACGACTTTGAACTCCCTCATTGAGAG
3' G12V Forward: AGTCGTGGTTCTTGGTTCAGTTGGTGTCGGAAAATCGGCG
3' G12V Forward: AGTCGTGGTTCTTGGTTCAGGAGGTGTCGGAAAAGCGGCG
3' Reverse: GATCCCCCGGGCTGCAGGAACGGCCAATTTGTCCCATTCC

rap-2 sequencing (1867bp)
Forward: GTCCTGCGCCCTTCTTTGTTCTG
Reverse: GGCTCGAATTTACCAGATTTTACG

RT-qPCR
rap-2
Forward: CGTTGACGGTGCAATTTGTCAG
Reverse: CCTGCAGTCTCCAGAATTTCCAC

cdc-42
Forward: CTGCTGGACAGGAAGATTACG
Reverse: CTCGGACATTCTCGAATGAAG

Repair template sequence

rap-2 G12V (miz16)
TAAAGATAGCTGCCCAAAAAATTTGCTACTCCACTTTAGAATCAATTTCAGCCTGAA
AACTTTTCAAATCCGAGGTTTTAATTTCAGTTTTCCTATTACTTTTCAACATCAAATT
GCCGAGAATGTTATAGCAATAATGAAATGAAAAAAGGAAGACGAACGAACGAGAA
ACAACAAAAAAAACTTTCACAATTTCCATTTCATTCATACCATCATCATCATCTCTTCA
AACTTCCGTTTCATTCTTTCCCATTTTTTCCGGTTATTGTTGTCTGTGTGTGTGGTG
ATGTAATAGTTCTACTACAATAATTCGTTCTTCTTCTTTTCTCACTTTTCCCACCACAT
TCACAATCACACCTAATCCAATTTATTGATTTTCAGCAAAAAACTCTCAATGAGGGA

GTTCAAAGTGGTCGTTCTGGGATCCGTTGGTGTCGGAAAATCGGCGTTGACGGTGCA
ATTTGTCAGTAGCACATTCATCGAGAAGTATGATCCGACGATTGAGGACTTTTATCG
CAAGGAAATTGAAGTGAGAGCGATTCATTTTATTTTAAATTTAAAAAAAAAAAAAG
AAAA

rap-2 G12V (miz17, miz18)

AGCTACGATCGCTCGTGTACTCCCCGAGGAGAAGGAGTTTACAGTTTTTCGTTAAAA
TGCTCGATTTTTGACTTTTTTTTGCAAATTCGTTCGGTATTCAACAGATTTTCTCTTTTT
TCCAGTTTTTTACAAGAAAACTGATGATTTTTTGATTAAAAACTACTGAAACCGATA
ATTTTTAGACTTTCGCCGAAAAACACATAGAATCCCCAAAAATCCTATAAACAAGAA
CTTTTATAGCTTTAAATACATGAAGAAGTAGTAAAAATGCTACAAAATCAAATATTG
TAGGAAAAAACTGTAAAATTCTTTTTCTCAGGGAGCAAGTAATGGGAGTTCTAAAAT
CTTTCAATTTCAAAGCTTAATATAATGTTTTAATGAATTTTTAGAAACTTTAAACCAT
TCTGAAAATTTCAAGCGCCATGATTTCAACCGAATTTTCTTTTTTTTTTTTTAAATTTA
AAATAAAATGAATCGCTCTCACTTCAATTTCCTTGCGATAAAAGTCCTCAATCGTCG
GATCATACTTCTCGATGAATGTGCTACTGACAAATTGCACCGTCAACGCCGATTTTC
CGACACCAACTGAACCAAGAACCACGACTTTGAACTCCCTCATTGAGAGTTTTTTGC
TGAAAATCAATAAATTGGATTAGGTGTGATTGTGAATGTGGTGGGAAAAGTGAGAA
AAGAAGAAGAACGAATTATTGTAGTAGAACTATTACATCACCACACACACACAGAC
AACAATAACCGGAAAAAATGGGAAAGAATGAAACGGAAGTTTGAAGAGATGATGA
TGATGGTATGAATGAAATGGAAATTGTGAAAGTTTTTTTGTTGTTTCTCGTTCGTTCG
TCTTCCTTTTTTCATTTCATTATTGCTATAACATTCTCGGCAATTTGATGTTGAAAAGT
AATAGGAAAACTGAAATTAAAACCTCGGATTTGAAAAGTTTTCAGGCTGAAATTGA
TTCTAAAGTGGAGTAGCAAATTTTTTGGGCAGCTATCTTTAGCTGAAATGTTCAAAT
TTGCCAACCTCTCAGAGCCACAACGGTCGAAAAATCAATATTTATGTATTAAAGCTC
CTTTGTTTTGCAAATTTCGGTCGTTTATATCTAATTTTTTGATAATTTAGGCACATTTT
CAGTCAATAGGTGTACAAACTAACAGAAAAATAATGTAAAAACTTTAGAAATCCTC
TAAACGAGACAGTAATTGGATAAATATTAATTCCGGCCGCTAGGAATGGGACAAAT
TGGCCG

rap-2 G12V (miz19, miz20)

AGCTACGATCGCTCGTGTACTCCCCGAGGAGAAGGAGTTTACAGTTTTTCGTTAAAA
TGCTCGATTTTTGACTTTTTTTTGCAAATTCGTTCGGTATTCAACAGATTTTCTCTTTTT
TCCAGTTTTTTACAAGAAAACTGATGATTTTTTGATTAAAAACTACTGAAACCGATA
ATTTTTAGACTTTCGCCGAAAAACACATAGAATCCCCAAAAATCCTATAAACAAGAA
CTTTTATAGCTTTAAATACATGAAGAAGTAGTAAAAATGCTACAAAATCAAATATTG
TAGGAAAAAACTGTAAAATTCTTTTTCTCAGGGAGCAAGTAATGGGAGTTCTAAAAT
CTTTCAATTTCAAAGCTTAATATAATGTTTTAATGAATTTTTAGAAACTTTAAACCAT
TCTGAAAATTTCAAGCGCCATGATTTCAACCGAATTTTCTTTTTTTTTTTTTAAATTTA
AAATAAAATGAATCGCTCTCACTTCAATTTCCTTGCGATAAAAGTCCTCAATCGTCG
GATCATACTTCTCGATGAATGTGCTACTGACAAATTGCACCGTCAACGCCGCTTTTC
CGACACCTCCTGAACCAAGAACCACGACTTTGAACTCCCTCATTGAGAGTTTTTTGC
TGAAAATCAATAAATTGGATTAGGTGTGATTGTGAATGTGGTGGGAAAAGTGAGAA
AAGAAGAAGAACGAATTATTGTAGTAGAACTATTACATCACCACACACACACAGAC
AACAATAACCGGAAAAAATGGGAAAGAATGAAACGGAAGTTTGAAGAGATGATGA
TGATGGTATGAATGAAATGGAAATTGTGAAAGTTTTTTTGTTGTTTCTCGTTCGTTCG

TCTTCCTTTTTTCATTTCATTATTGCTATAACATTCTCGGCAATTTGATGTTGAAAAGT
AATAGGAAAACTGAAATTAAAACCTCGGATTTGAAAAGTTTTCAGGCTGAAATTGA
TTCTAAAGTGGAGTAGCAAATTTTTTGGGCAGCTATCTTTAGCTGAAATGTTCAAAT
TTGCCAACCTCTCAGAGCCACAACGGTCGAAAAATCAATATTTATGTATTAAAGCTC
CTTTGTTTTGCAAATTTCGGTCGTTTATATCTAATTTTTTGATAATTTAGGCACATTTT
CAGTCAATAGGTGTACAAACTAACAGAAAAATAATGTAAAAACTTTAGAAATCCTC
TAAACGAGACAGTAATTGGATAAATATTAATTCCGGCCGCTAGGAATGGGACAAAT
TGGCCG